Universitat Politècnica de Catalunya
Escola Tècnica Superior d'Enginyeria de Camins, Canals i Ports

Departament de Matemàtica Aplicada III

Numerical Simulation of Fast Transient Phenomena in Fluid-Structure Systems

by

Beñat Oliveira Bravo

Master Thesis
Advisor: Pedro Díez

Barcelona, June 2012

Abstract

Numerical Simulation of Fast Transient Phenomena in Fluid-Structure Systems

Beñat Oliveira Bravo

In this master thesis the Fast Transient Fluid-Structure interaction is studied. The goal is to understand the numerical methods behind the models that simulate this phenomena, in order to be able to reproduce them in two examples.

First, the numerical analysis and the equations behind are described and understood in terms of structural domain, the fluid and their interaction. Here, both the problem statement and the numerical approach are deeply developed. Then, specific strategies are explained in order to apply them in the proposed examples.

Two examples are presented to clarify the explanations and strengthen the knowledge in the subject. The numerical examples are thoroughly studied in order to illustrate the functioning of the EUROPLEXUS code and the limits of the method. Firstly, the structural damage under dynamic loads induced by explosions are analyzed, towards different models and approaches. Mesh refinement is compared, and the influence of certain factors highlighted concerning FEM. In the second simulation, an steel-made water tank has been tested for a projectile shoot. For this, the SPH method has been used.

Acknowledgments

En primer lugar, gracias a Francesc por haberme ayudado miércoles tras miércoles en ese laboratorio del C2. De la misma manera agradecer la predisposición de Pedro y Folco Casadei en resolver lo imposible. Eskerrik asko hiruoi.

No podría seguir sin una mención especial a Rosa Estela. Algún día devolveré parte de lo que me has enseñado, y me responderás en euskera.

A tots aquells que me heu suportat durant aquests curts cinc anys. Julen eta Sara ni hona ekarri izanagatik. Txonpio, Arantza, zuei ere eskerrak. Av. Sarrià 37 i 39. Vosaltres heu estat la universitat de veritat, on he sigut feliç. Dani, Pau, Oriol y Xesc; gràcies per fregar els meus plats. Sector camins, Aribau 123 4.2, Punta Cana y Centre de Càlcul. A vosaltres també gràcies per fer-ho tot més fàcil.

Donostin besoak zabalik jasotzen nauzuen guztioi. Nitaz ahaztu ez eta zaudeten lekuan zaudetela zuen itzalpeko lagun honekin kontatzeagatik. 3 urtetatik 23 urtetara. Gora Monaluixa! Eskerrik asko eta laster arte.

Eta, azkenik esker mila familiari, etxeko lauoi. Ezer ez litzateke posible izango zuek gabe. Ibon, ea noizbait zure laurdenera iristen naizen. Aita eta ama, hitzik ez.
Oso harro nago zuetaz. Ez dakizue zuek zenbat.

"Ver, oir y callar..."
Ángel Oliveira Lassalle

Contents

List of Figures

List of Tables

Chapter 1

Introduction

1.1 Motivation

Explosions, crashes, hits, earthquakes, gas accidents... all of this dynamics actions have something in common: the small time interval in which they happen. This fast Transient Dynamic Phenomenons usually involve more than one agent so whole Fluid-Structure Systems are needed so as to represent the reality. Industries are very interested on those types of hazard simulations, as a great amount of information could be obtained anywhere, anytime, and what is more important, without any material or personal looses.

Nowadays, everybody cares about the security. The historical context in which we live requires the authorities to invest in this issue. Recent terrorists attacks have been modeled and numerically simulated, and huge advances have been done with them. New software has been developed and the application spectrum widely spread. The Fast Transient Fluid Structure Interaction is used in the analysis civil engineering common problems (earthquakes, soil-structure interaction, building vulnerability...), in the energy sector (nuclear and fossil-fueled plants, electrical devices...), marine/offshore industry, transportation and everywhere imaginable.

This document is part of the ongoing collaboration between the LaCaN and the Institute for the Protection and Security of the Citizen (IPSC) part of the Joint Research Center (JRC) of the European Commission. Three decades of code development (EUR-DYN, Castem-PLEXUS/PLEXIS-3C) have lead to the creation of the EUROPLEXUS, a is general Finite Element software for the non-linear dynamic analysis of Fluid-Structure systems subjected to fast transient dynamic loading. LaCaN research fields are mainly upstream, working on the theorical basis of the code such as adaptivity.

So, lots of applications, lots of open gates. This document is my first approach towards this sector, a first step that encourages me to follow studying once finished this master thesis in Barcelona.

(a) Reality (b) Model

Figure 1.1: 11-M numerical simulation.

1.2 Aims and goals

This document aims to follow the collaborative task described above, testing the potential capabilities of the EUROPLEXUS, and the constructing two synthetic examples. The objectives behind are the following:

- Understand and become confident with the EUROPLEXUS code, as well as the numerical component and the equation's treatment.
- Test the potential capabilities of the EUROPLEXUS, applying and developing two synthetic examples of interest in two different numerical approaches. In addition, the obtained results are compared with the reality and their reliance and utility discussed. The developed examples are the following:
  - Structural failure under explosion with FEM.
  - Firing a projectile against a metal tank filled with water, by SPH method.

Chapter 2

Structural Modeling

2.1 Problem Statement

In this section the main equations are going to be defined, in order to treat them with numerical methods in the next one. This mathematical first approach describes the behavior of the solid in equilibrium with some external forces.

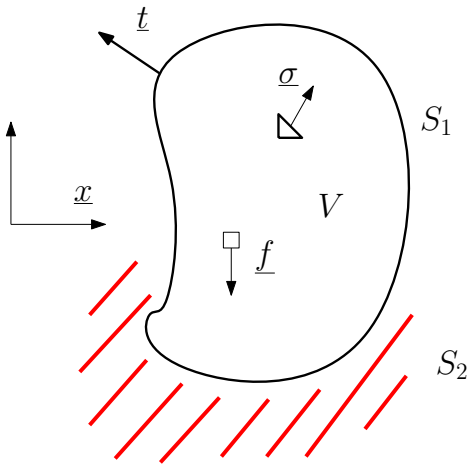

Figure 2.1: System description.

The structural domain is governed by the principle of virtual work. This equation represents the conservation of momentum, which means the common equilibrium but in a dynamic sense.

$$\int_V \rho \underline{\ddot{x}} \partial \underline{x} dV + \int_V \underline{\sigma} D(\partial \underline{x}) dV - \int_V \rho \underline{f} \partial \underline{x} dV - \int_{S_1} \underline{t} \partial \underline{x} dS = 0 \tag{2.1}$$

Where each coefficient means:

ρ mass density	$\underline{\sigma}$ Cauchy stress
V current domain	D spatial derivative operator
$\underline{x}$ current configuration	$\underline{f}$ volumetric forces per unit mass
$\underline{\ddot{x}}$ accelerations	$\underline{t}$ boundary surface traction

On the other hand the constitutive law has to be fixed for each material. This constitutive law has to deal with large motions and rotations, so both geometrical non-linearities and material non-linearities may occur. For a general approach it can be defined as a function f_r dependent of a displacement:

$$\sigma = f_r(x - x_0) \tag{2.2}$$

The whole system must hold for all variations ∂x of configuration (virtual displacements) compatible with essential boundary conditions on S_2. A suitable numerical method is required to solve those equations and describe the structural motion in every time step.

2.2 Numerical method

This integral form (2.1) lends itself to direct application of FE method. The following spatial discretization is used (2.3).

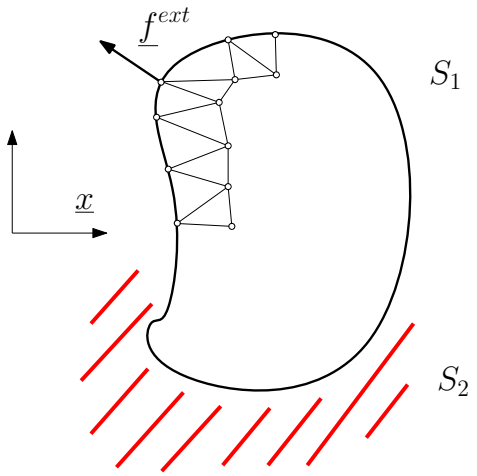

Figure 2.2: System description for FE.

$$\underline{M\ddot{u}} = \underline{f}^{ext} - \sum_e \int_{V^e} \underline{B}^t \underline{\sigma} dV \tag{2.3}$$

Where each coefficient means:

$\underline{M}$ mass matrix	$\sum_e$ standard FE assembly operator
$\underline{u}$ nodal displacement vector	V^e element e current volume
$\underline{f}^e xt$ discrete external forces	$\underline{B}$ matrix of shape functions derivatives

The external forces are computed in the nodes and $\sum_e$ gathers the information about the neighbors' elements in a discrete node. This set of discrete differential equations in time is decoupled by diagonalization (lumping) of the mass matrix $\underline{M}$.

The computational framework has its own characteristics. Here you have a first collection of them:

- Lagrangian description. The mesh remains associated with the same material point. The nodes and Gauss Points always "follow" the particles.
- Stress is "true". It is normally expressed in a fixed reference in the space.
- All RHS terms[1] are known or computable. The stresses must be obtained via material constitutive law (2.2).
- Diagonalization of $\underline{M}$ by lumping.

$$\underline{M}^e = \int_{V^e} \underline{N} \rho dV \tag{2.4}$$

  Where $\underline{N}$ are the element shape functions.

- The structural behavior is defined in the current configuration. There is no need to define a reference configuration. In addition, the total deformation is not used.

2.2.1 FEM for structural domain

The most "natural" description for the structural domain is the *Lagrangian description* (see figure 2.3) used within FE. The referential domain is attached to material particles during the whole computation. This means that the mesh follows the motion of the structure, and its deformation is directly linked with the material expansion or contraction.

2.2.2 Explicit time integration scheme

There are different ways to deal with the time integration. The next step is to define an effective time integration scheme. The accuracy and stability should be checked, as well as its the conditional behavior concerning the elements' length or even the material characterization. Every question related with the general integration pattern will be answered and

[1] $\underline{f}^{ext}$, $\underline{B}$

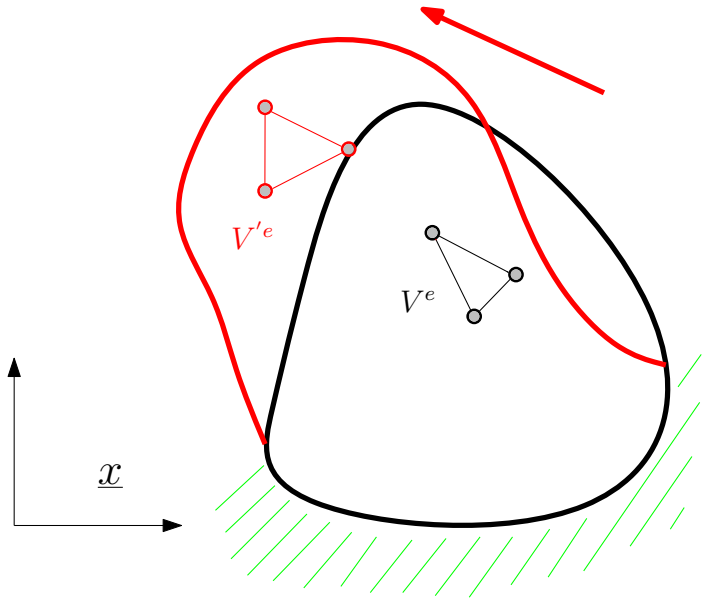

Figure 2.3: Bar element.

explained in this section.

Direct Time Integration

Time integration is achieved via the Central Difference scheme [4], usually written as[2] (2.5):

$$\underline{\dot{u}}^{n+1} = \underline{\dot{u}}^{n} + \frac{\Delta t}{2}(\underline{\ddot{u}}^{n} + \underline{\ddot{u}}^{n+1}) \tag{2.5a}$$

$$\underline{u}^{n+1} = \underline{u}^{n} + \Delta t \left(\underline{\dot{u}}^{n} + \frac{\Delta t}{2}\underline{\ddot{u}}^{n} \right) \tag{2.5b}$$

Where,

$$n \text{ stays for time } t^n$$

$$n+1 \text{ stays for } t^{n+1} = t^n + \Delta t$$

$$\Delta t \text{ is the time increment}$$

[2]These formulas are a particularization of the Newmark integration formulas [5]:

$$\underline{\dot{u}}^{n+1} = \underline{\dot{u}}^{n} + \Delta t[(1-\gamma)\underline{\ddot{u}}^{n} + \gamma\underline{\ddot{u}}^{n+1}]$$

$$\underline{u}^{n+1} = \underline{u}^{n} + \Delta t\underline{\dot{u}}^{n} + \frac{\Delta t^2}{2}[(1-2\beta)\underline{\ddot{u}}^{n} + 2\beta\underline{\ddot{u}}^{n+1}]$$

written for $\gamma = 1/2$ and $\beta = 0$

These two equations, plus the equilibrium[3], can be solved for $\underline{u}$, $\underline{\dot{u}}$, $\underline{\ddot{u}}$ upon step-by-step marching in time. This particular choice for β renders the scheme explicit, while the chosen γ ensures no numerical damping.

There is some trouble in using this scheme in practice, so a little implementation guide is shown below.

1. Introduction of a mid-step velocity.

$$\underline{v}^{n+1/2} = \underline{\ddot{u}}^n + \frac{\Delta t}{2}\underline{\ddot{u}}^n \tag{2.7}$$

   this transforms n into $n+1$ over the step.

2. The second equation (2.5) becomes:

$$\underline{u}^{n+1} = \underline{u}^n + \Delta t \underline{v}^{n+1/2} \tag{2.8}$$

3. Another mid-step velocity must be computed so as to restart the buckle. The first equation (2.5) becomes:

$$\underline{v}^{n+3/2} = \underline{v}^{n+1/2} + \Delta t \underline{\ddot{u}}^{n+1} \tag{2.9}$$

$$\underline{v}^{n+3/2} = \underline{\dot{u}}^{n+1} + \frac{\Delta t}{2}\underline{\ddot{u}}^{n+1} = \underline{\dot{u}}^n + \frac{\Delta t}{2}\underline{\ddot{u}}^n + \frac{\Delta t}{2}\underline{\ddot{u}}^{n+1} + \frac{\Delta t}{2}\underline{\ddot{u}}^{n+1} = \underline{v}^{n+1/2} + \Delta t \underline{\ddot{v}}^{n+1}$$

So the algorithm is based on a mid-step velocity rather than full-step one. As shown a new configuration is obtained first. Then, on this known configuration, equilibrium is enforced (2.3). The new mid-step velocity is obtained last[4]. Nevertheless, the acceleration in the step $n+1$, $\underline{\ddot{u}}^{n+1}$, needs a further explanation, and this document comes back to this topic later (section 2.2.3).

This scheme is completely explicit and needs no iteration to keep on working. Notice that the time step Δt has been treated as fixed, but this does not always happen, as it is not mandatory. If Δt varies in time, the only change is in the equation (2.9), which becomes:

$$\underline{v}^{n+3/2} = \underline{v}^{n+1/2} + \frac{\Delta t^n + \Delta t^{n+1}}{2}\underline{\ddot{u}}^{n+1} \tag{2.10}$$

[3]Equilibrium equation:

$$\underline{M\ddot{u}} = \underline{f}^{ext} - \underline{f}^{ext} \tag{2.6}$$

[4]Europlexus also computes the full-step velocities:

$$\underline{\dot{u}}^{n+1} = \underline{v}^{n+1/2} + \frac{\Delta t}{2}\underline{\ddot{u}}^{n+1}$$

These are the velocities printed out in the listing and visualized in post-processing.

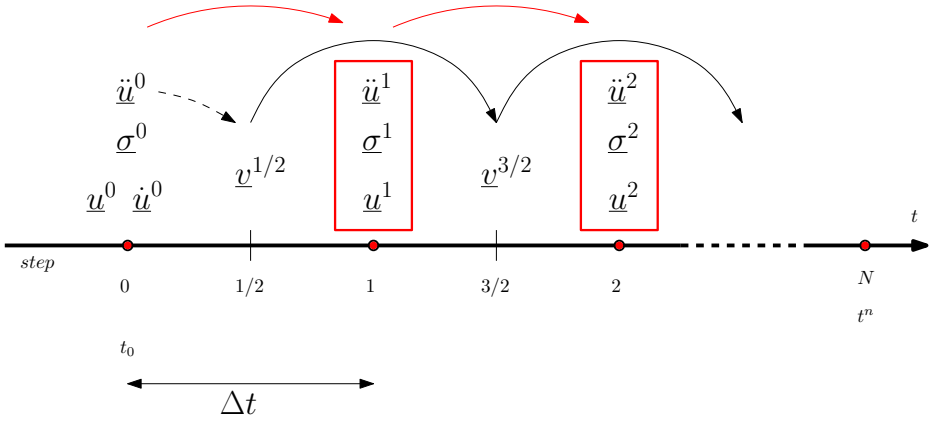

Figure 2.4: Scheme start-up and marching.

with,

$$\Delta t^n \equiv t^{n+1} - t^n$$
$$\Delta t^{n+1} \equiv t^{n+2} - t^{n+1}$$

Time Integration Scheme Characteristics

Central difference scheme [4] has second-order accuracy and introduces no numerical dumping. However, CD is conditionally stable and it depends on Courant's number (figure (2.5)). It compares the length of the element with the light's speed as :

$$\Delta t^e_{stab} \approx \frac{L^e}{c^e} \tag{2.11}$$

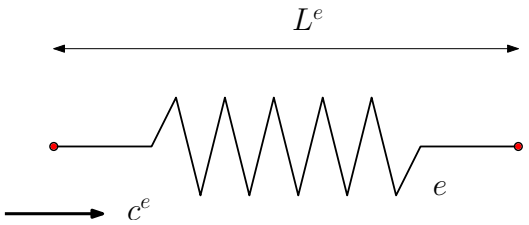

Figure 2.5: Stability depending on element's length and light's speed.

It is convenient to choose a slightly inferior time step so as to prevent from an unstable condition. That is why the selected time step is the one which ensures stability multiplicated

by a safety coefficient ($\varphi < 1$):

$$\Delta t^e = \varphi \Delta t^e_{stab} \tag{2.12}$$

Spectral analysis shows that the CD scheme tends to produce frequencies slightly higher than physical ones. Same effect is obtained using a consistent mass matrix. On the other hand, the use of a lumped mass matrix tends to reduce frequency values. Therefore, combination of CD time integrator with a lumped mass matrix gives optimal numerical precision.

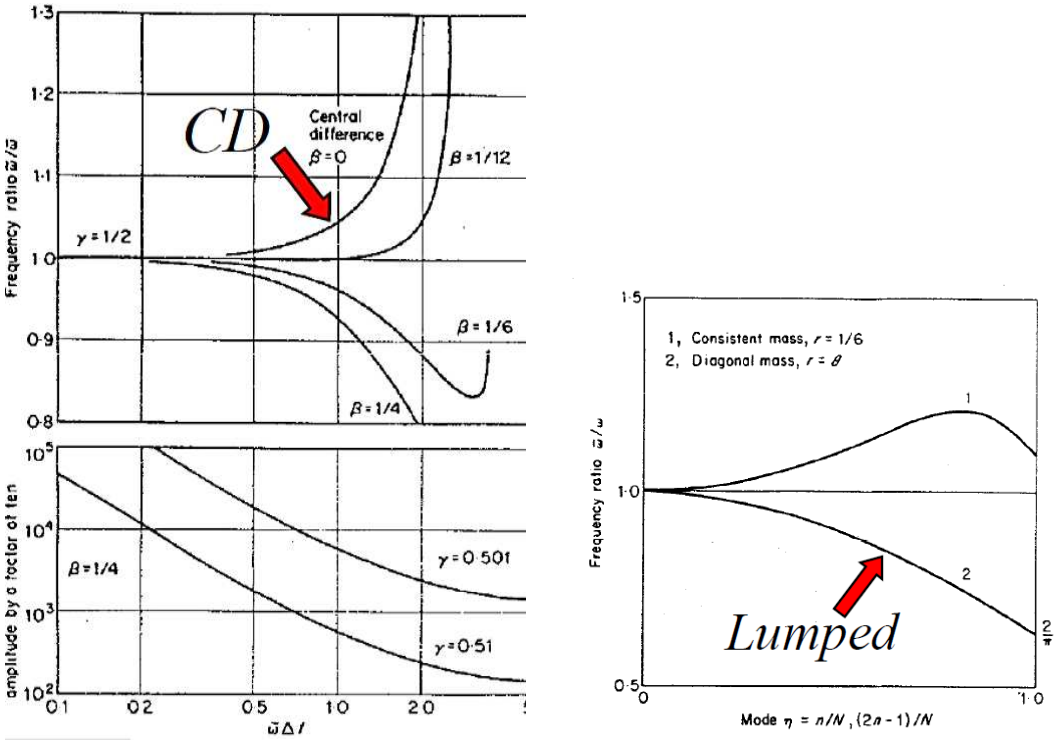

(a) Scheme (b) Mass Matrix

Figure 2.6: Scheme and Mass Matrix effect on frequency [1].

The previous result is highly remarkable, since the final equations are completely decoupled: just the opposite to classical FE method, there are no matrices to assemble and no need for system solvers with the exception of the treatment of some essential boundary conditions.

2.2.3 Integration of the Constitutive law

The stress information must be updated in every single step as shown in the equilibrium equation (2.3). The new stress $\underline{\sigma}^{e(n+1)}$ is needed to compute the new acceleration $\underline{\ddot{u}}^{n+1}$ and it is commonly got from the constitutive law. The constitutive law vary with the material, but without los of generality, the following can be written.

$$\underline{\sigma}^{n+1} = \underline{\sigma}^{n} + \Delta\underline{\sigma}^{n} \tag{2.13}$$

$$\Delta\underline{\sigma} = H(\underline{\sigma}^{n}, \Delta\underline{\varepsilon}, \underline{p}, \dot{\underline{\varepsilon}}, ...) \tag{2.14}$$

H constitutive law
$\Delta\underline{\sigma}$ stress increment over the step — $\underline{p}$ hardening parameters (e.g. plasticity)
$\Delta\underline{\varepsilon}$ strain increment over the step — $\dot{\underline{\varepsilon}}$ strain rate (e.g. viscous behavior)

Note that the total deformation $\underline{\varepsilon}$ does not appear anywhere and that it is not used in the process.

As an example of non-linear material behavior consider the important case of metal plasticity. Rate-independent deviatoric plasticity model with Von Mises yield is generally the model choused:

$$\underline{\sigma}_{n+1}^{trial} = \underline{\sigma}_{n} + \underline{\underline{C}}\Delta\dot{\underline{\varepsilon}} \tag{2.15}$$

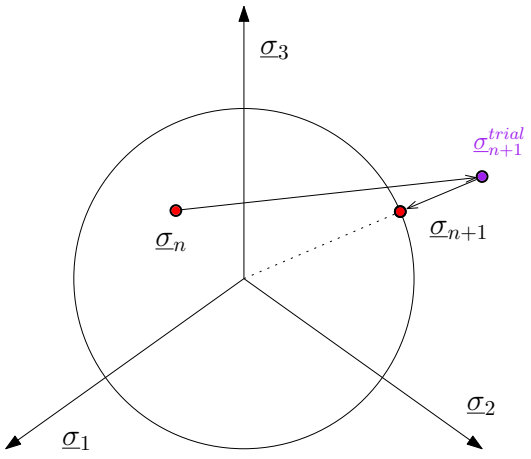

Figure 2.7: Radial return method in Von Mises.

To compute the new stress the radial return method is held. The first step requires a new trial stress, $\underline{\sigma}_{n+1}^{trial}$. If this new point is inside the Von Mises yield volume the scheme keeps on working with $\underline{\sigma}_{n+1} = \underline{\sigma}_{n+1}^{trial}$ and there is no extra complication. But if the trial point lies in the outside, the Wilkin's method [6] (figure (2.7)) projects the $\underline{\sigma}_{n+1}^{trial}$ into the yield surface in a direct way with no iterations.

There is another fact that one should take into account: *the geometrical non-linearities*. This turns the computation of $\Delta\underline{\varepsilon}$ required in the equation (2.15) a little bit tricky as large strains and large motions appear, specially large rotations. Literature explains different ways to solve this problem, but a large-displacement/large-strain formulation is adopted for full generality and the constitutive law (2.2) turn non-linear.

The work scheme can be reduced in 3 fases for continuum-like FE:

1. First of all, the spatial velocity gradient must be computed.

$$\underline{L} = \partial\dot{\underline{x}}/\underline{x}$$

2. Then an additive decomposition is used to separate instantaneous deformation (symmetric) from rotation (antisymmetric part).

$$\underline{L} = \underline{D} + \underline{W}$$

$$\underline{D} = \frac{1}{2}\left(\underline{L} + \underline{L}^T\right) \text{ stretching}$$

$$\underline{W} = \frac{1}{2}\left(\underline{L} - \underline{L}^T\right) \text{ spin}$$

3. Finally, $\Delta\underline{\varepsilon}$ is obtained as:

$$\dot{\underline{\varepsilon}} = D \quad ; \quad \Delta\underline{\varepsilon} = \underline{D} \cdot \Delta t$$

For a continuum the state of the stress of interest to us, Cauchy stress $\underline{\sigma}$, is referred to a fixed frame in the space. Consequently, its time derivative is not invariant with respect to rotation, so $\dot{\underline{\sigma}}$ is not objective.

An objective rate of the stress $\widehat{\underline{\sigma}}$ can be obtained under the form $\widehat{\underline{\sigma}} = \dot{\underline{\sigma}} - \underline{A\sigma} + \underline{\sigma A}$ where $\underline{A}$ is an appropiate vorticity matrix[5]. However, the those considerations are valid only in an infinitesimal sense, while finite increments are needed in those fast-transient phenomena. An incrementally objective scheme must been set up to update the Cauchy stress. For a 2D case, the scheme is divided in three phases, where α is the rotation over Δt and $\theta = \alpha/2$.

[5] In the Zaremba-Jaumann-Noll formulation [7] $\underline{A} = \underline{W}$. Other choices are possible, such as Green-Naghdi [8].

1. Firstly, the first half of the rotation increment is applied (2.16).

$$\underline{\sigma}^{\hat{n}} = \underline{R}\underline{\sigma}^{n}\underline{R}^{T} \tag{2.16}$$

$$\text{with} \quad R = \begin{bmatrix} \cos\theta & \sin\theta \\ -\sin\theta & \cos\theta \end{bmatrix}$$

2. Then, the constitutive equation is applied:

$$\underline{\sigma}^{n\hat{+}1} = \underline{\sigma}^{\hat{n}} + \underline{\underline{C}} \cdot \Delta t \cdot \underline{D}^{n+1/2} \tag{2.17}$$

3. Finally, the second half of the rotation increment is computed:

$$\underline{\sigma}^{n+1} = \underline{R}\underline{\sigma}^{n\hat{+}1}\underline{R}^{T} \tag{2.18}$$

For structural elements (bars, beams, shells) the co-rotational formulation is used. Here the stress is measured in a reference frame that rotates with the element. This greatly simplifies the stress increment procedure, as the stress can be incremented directly by applying the constitutive law. For a bar element for instance, the strain can be treated in a natural or logarithmic strain, or even with a small-strain formulation.

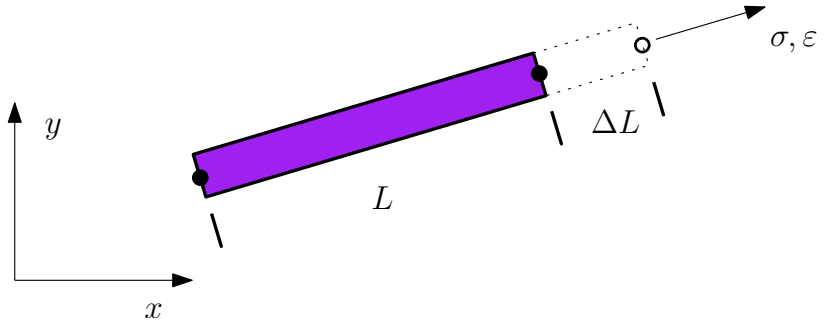

Figure 2.8: Bar element.

Natural or logarithmic strain

$$\Delta\varepsilon = \frac{\Delta L}{L} \quad \rightarrow \quad \Delta\sigma \tag{2.19}$$

$$\sum \Delta\varepsilon = \sum \frac{\Delta L}{L} \simeq \int_{L_0}^{L} \frac{dL}{L} = ln\frac{L}{L_0} \tag{2.20}$$

Engineering strain

$$\Delta\varepsilon = \frac{\Delta L}{L_0} \quad \rightarrow \quad \sum \Delta\varepsilon = \frac{L - L_0}{L_0} \tag{2.21}$$

Advantages of the method

To sum up, the transient dynamic problem finds out $\underline{\sigma}$ on new configuration $\underline{x}$ (known) from $\underline{\sigma}^{old}$ and the deformation process between $\underline{x}^{old}$ and $\underline{x}$. This technique is especially powerful in comparison with the implicit methods. The implicit methods find $\underline{\sigma}$ and $\underline{x}$ simultaneously, typically by iterative procedures and convergence criteria. On the contrary, an explicit scheme avoids the calculation of every mid-steps. In addition, the proposed method is particularly simple for complex non-linear problems, hence very robust.

Furthermore, direct application of virtual work principle (2.1) plus second order accurate time integration scheme (2.5), guarantee high accuracy of numerical results.

2.2.4 Solution's verification

The quality of the obtained numerical results must be checked somehow, and this can be done by computing at each time step the *energy balance*. The general process carried out is described below.

- Initially, the external work, W_0^{ext}, is set:

$$W_0^{ext} = E_0^{int} + E_0^{kin} \tag{2.22}$$

- At any time, the balance error can be computed as:

$$\varepsilon = \frac{W^{ext} - \left(E^{int} + E^{kin}\right)}{W_0^{ext}} \tag{2.23}$$

  or perhaps better,

$$\varepsilon = \frac{W^{ext} - \left(E^{int} + E^{kin}\right)}{max\left(|W^{ext}|, |W_0^{ext}|\right)} \tag{2.24}$$

This error indicator is used a posteriori in order to check the previous time-step solution, and must not be confused with convergence parameters, typical from iterative approaches.

2.2.5 Implementation of Boundary conditions

In this section the imposition of the essential boundary conditions is going to be analyzed. The code treats them via *Lagrange multipliers* although first some assumptions must be

done concerning the constraints. The code needs to assume the imposed restrictions and in a second step express the unknown reactions via Lagrange multipliers.

- First, it is assumed a linear set of constrains on the velocities:

$$\underline{\underline{C}}\underline{v} = \underline{b} \tag{2.25}$$

  Both $\underline{\underline{C}}$ and $\underline{b}$ are known, and can be function of time.

- The equilibrium equation (2.6) presented before is modified so as to take into account the reactions:

$$\underline{ma} = \underline{f}^e - \underline{f}^i + \underline{r} \tag{2.26}$$

- Without loss of generality, the unknown reactions can be expressed via a vector $\underline{\lambda}$ of Lagrange multipliers:

$$\underline{r} = \underline{\underline{C}}^T \underline{\lambda} \tag{2.27}$$

The Lagrange multipliers method

The reactions can be expressed by the Lagrange Multipliers (2.27) and this structure be replaced in the equilibrium equation (2.26) as shown in (2.28).

$$\underline{ma} = \underline{f}^e - \underline{f}^i + \underline{\underline{C}}^T \underline{\lambda} \tag{2.28}$$

Multiplying both members by $\underline{\underline{C}}\underline{m}^{-1}$ gives:

$$\underline{\underline{C}}\underline{a} = \underline{\underline{C}}\underline{m}^{-1}\left(\underline{f}^e - \underline{f}^i\right) + \underline{\underline{C}}\underline{m}^{-1}\underline{\underline{C}}^T\underline{\lambda} \tag{2.29}$$

Where $\underline{B}^* = \underline{\underline{C}}\underline{m}^{-1}\underline{\underline{C}}^T$ is the matrix of connections. The Lagrange multipliers are obtained symbolically from (2.29), $\underline{B}^*\underline{\lambda} = \underline{\underline{C}}\underline{a} - \underline{\underline{C}}\underline{m}^{-1}\left(\underline{f}^e - \underline{f}^i\right)$. To get λ, the term $\underline{\underline{C}}\underline{a}$ must be expressed as a function of known quantities, by using the constraints and time integration scheme. From the CD scheme for the velocity (2.9), imposing a constant Δt and substituting this into the constraints $\underline{\underline{C}}\underline{v} = \underline{b}$ (2.25) gives[6]:

$$\underline{\underline{C}}\underline{v}^{n+3/2} = \underline{\underline{C}}\underline{v}^{n+1/2} + \Delta t \cdot \underline{\underline{C}}\underline{a}^{n+1} = b \tag{2.30}$$

Reordering the terms $\underline{\underline{C}}\underline{a}$ can be easily obtain as:

$$\underline{\underline{C}}\underline{a} = \frac{1}{\Delta t}\left(\underline{b} - \underline{\underline{C}}\underline{v}^{n+1/2}\right) = \frac{1}{\overline{\gamma}}\left(\underline{b} - \underline{\underline{C}}\underline{v}^{n+1/2}\right) \tag{2.31}$$

[6]Notice the different notation but same meaning of the acceleration:

$$\underline{\ddot{u}} = a$$

This analysis has been done for $\overline{\gamma} = \Delta t$ constant in time, but it can be expanded for a variable Δt in time, by doing this simple trick:

$$\overline{\gamma} = \frac{\Delta t^n + \Delta t^{n+1}}{2} \tag{2.32}$$

Summarizing, the Lagrange Multipliers $\underline{\lambda}$ are obtained by solving the linear algebraic system $\underline{B}^*\underline{\lambda} = \underline{w}$ where the known terms are given by $\underline{B}^* = \underline{Cm}^{-1}\underline{C}^T$ and $\underline{w} \equiv \frac{1}{\overline{\gamma}}\left(\underline{b} - \underline{Cv}^{n+1/2}\right) - \underline{Cm}^{-1}\left(\underline{f}^e - \underline{f}^i\right)$. Finally the reactions are computed by $\underline{r} = \underline{C}^T\underline{\lambda}$ and added them to the other known external forces. A unique multiplier is obtained for each imposed constraint, and one reaction also for each constrain. Obviously a solver must be run to get those multipliers so this is the only implicit part of the whole method.

Chapter 3

Fluid Formulation

3.1 Introduction

The fluid's treatment is relatively new in comparison with its colleague, the structural material. But recent researchers are focusing on the behavior of the fluid and great improvements have been made concerning the numerical modelization and discretization of the fluid domain. This section discusses different ways of dealing with the fluids, and the one used by the code is going to be described deeply. The interaction between the fluid and structures comes later, so this formulation does not take into account a hypothetical "rigid" boundary.

3.2 Problem Statement

3.2.1 First Assumptions

First of all, some primal assumptions. Those points are basics in order to understand the coming hypothesis regarding the fluid (figure 3.1), and to know what type of problems can be solved with the code.

- The fluid is assumed to be compressible and inviscid. Viscous forces are negligible comparing them with high pressures, high pressure gradients and the computed inertial forces. Remember that the code has been thought to simulate fast dynamics phenomena, meanly those generated by high changes in pressure, such as explosions or air-blasts.
- The governing equations are the Euler equations, which express the conservation of mass, momentum and energy.
- The fluid's state equation must be taken into account during the calculation.

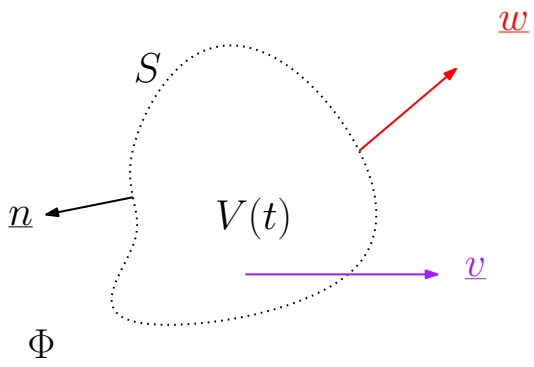

Figure 3.1: Fluid representation.

Φ = Fluid domain	$\underline{n}$ =unit normal
$V(t)$ = control volume	$\underline{v}(\underline{x}, t)$ = fluid velocity (particles)
$S(t)$ = control surface	$\underline{w}(\underline{x}, t)$ = arbitrary velocity (mesh)

3.2.2 Euler Equations

The governing Euler equations are the followings: *mass* (3.1), *momentum* (3.2) and *energy* (3.3). Those equations plus the fluid's equation of state rule the behavior of the fluid.

$$\frac{dM}{dt} \equiv \frac{d}{dt}\int_{V(t)} \rho dV = \oint_{S(t)} \rho\left(\underline{w} - \underline{v}\right) \bullet \underline{n} dS \tag{3.1}$$

$$\frac{d\underline{Q}}{dt} \equiv \frac{d}{dt}\int_{V(t)} \rho \underline{v} dV = \oint_{S(t)} \rho \underline{v}\left(\underline{w} - \underline{v}\right) \bullet \underline{n} dS - \int_{V(t)} \nabla p dV + \int_{V(t)} \rho \underline{g} dV \tag{3.2}$$

$$\frac{dE}{dt} \equiv \frac{d}{dt}\int_{V(t)} \rho e dV = \oint_{S(t)} \rho e\left(\underline{w} - \underline{v}\right) \bullet \underline{n} dS - \oint_{S(t)} p\underline{v} \bullet \underline{n} dS + \int_{V(t)} \rho \underline{g} \bullet \underline{v} dV \tag{3.3}$$

M = mass of control volume	ρ = fluid density	e = total specific energy
$\underline{Q}$ = momentum of control vol.	p = pressure	$\underline{\nabla}$ = gradient operator
E = energy of control vol.	$\underline{g}$ = gravity	$\bullet$ = scalar product

As mentioned, there is also a suitable equation of state depending on the fluid. This equation is necessary so as to solve the euler equations, as it describes the pressure as a function of the fluid's variables.

$$p = P(\rho, i) \tag{3.4}$$

For a compressible fluid, the total specific energy is (i = internal specific energy):

$$e = i + \frac{1}{2}v^2 \tag{3.5}$$

Finally, concerning the Euler formulas, another variation of the energy formula may be used. This new approach consists on replacing the total specific energy (3.5) with the internal energy form, I, and the equation (3.3) becomes:

$$\frac{dI}{dt} \equiv \frac{d}{dt}\int_{V(t)} \rho i dV = \oint_{S(t)} \rho i \left(\underline{w} - \underline{v}\right) \bullet \underline{n} dS - \int_{V(t)} p\underline{\nabla} \bullet \underline{v} dV \tag{3.6}$$

3.3 Numerical Method

In purely fluid problems, an *Eulerian description* is often more intuitive (figure 3.2). The referential domain, the mesh, is fixed in the space, and the fluid flows from one element to another. The fluid particles are not attached anymore to the mesh.

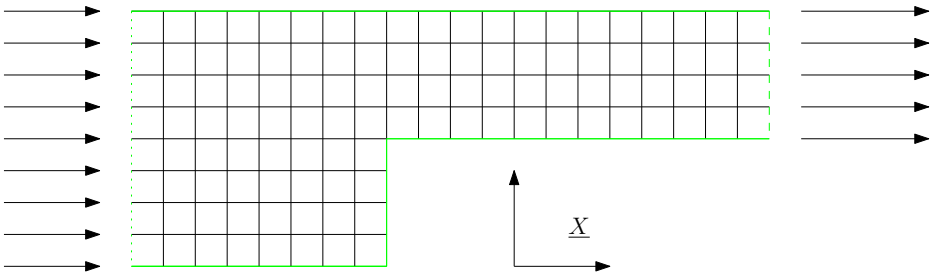

Figure 3.2: Eulerian

In problems involving both structures and fluids, a mixed description (ALE) can bring substantial benefits (figure 3.3). The referential domain is arbitrarily moving depending on the proximity of the structure.

The ALE description is a generalization of the Lagrangian and Eulerian descriptions. The figure 3.6 illustrates the difference between the three descriptions on a node-by-node basis.

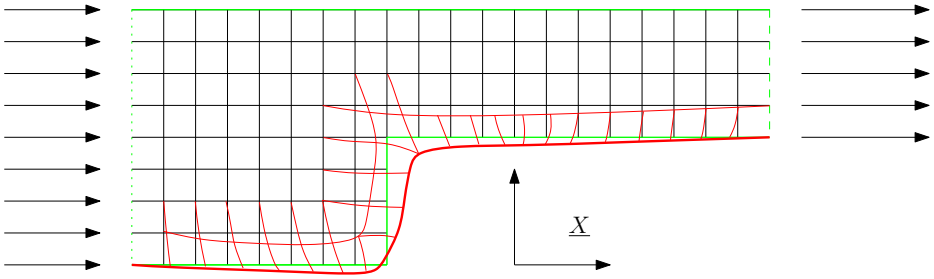

Figure 3.3: ALE

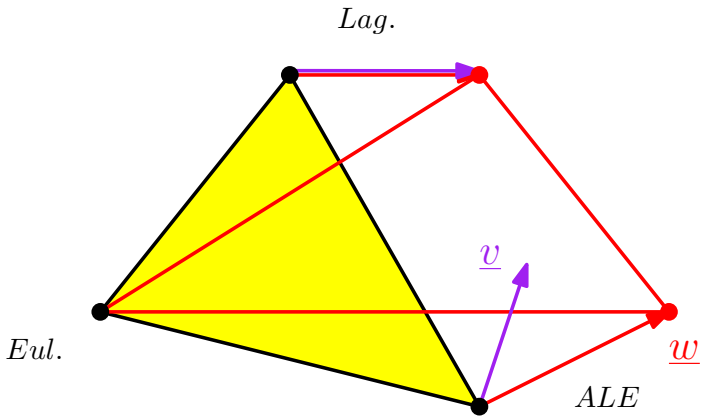

Figure 3.4: Comparison of Lagrangian, Eulerian and ALE descriptions.

- When $\underline{w} \equiv \underline{v}$ the description is Lagrangian.
- When $\underline{w} \equiv \underline{0}$ the description is Eulerian.
- Else, the description is ALE

Since $\underline{w}$ is arbitrary, it must be provided either by user or via suitable automatic rezoning algorithms.

3.3.1 Finite Element Discretization

In the examples tested in this minor thesis, the calculation has been carried out by Finite Elements (FE). In this case, the discretization goes via linear elements with velocities at nodes. ρ and i (hence p (3.4)) are uniform over each element, and integral forms off mass (3.1) and energy conservation (3.3) can be used directly for a given $V(t)$ (current element volume). But, on the other hand, the conservation of momentum (3.2) is more complex and requires a further treatment.

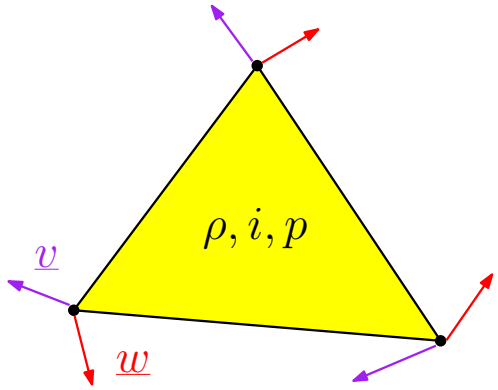

Figure 3.5: Finite element example, with velocities at nodes.

Treatment of Momentum Equation The previous integral statement (3.2) is unable to furnish enough equations, since the velocity field in each element depends upon $N \cdot d$ parameters (N being the number of nodes and d the space dimension). So, a variational statement associated with the differential form of the momentum equation may be formulated. As a final result, the *principle of virtual power*[1] appears:

$$\int_{V(t)} \Delta v_i \rho \frac{\partial v_i}{\partial t} dV = \int_{V(t)} \delta v_i \rho \left(\underline{w} - \underline{v}\right) \cdot \underline{\nabla} v_i dV + \int_{V(t)} \Delta v_i \rho g_i dV + \int_{V(t)} p \frac{\partial \left(\Delta v_i\right)}{\partial x_i} dV + \oint_{S(t)} \Delta v_i T_i dS \tag{3.7}$$

v_i are the components of fluid velocity $\underline{v}$

δv_i are arbitrary admissible variations of the fluid velocity

g_i are the components of the acceleration of the gravity

T_i are the components of prescribed boundary loads per unit area

x_i are the spatial coordinates (current position of particles in a fixed frame)

Time Integration
Each time increment is split into three phases:

1. *Explicit Lagrangian phase* By posing $\underline{w} = \underline{v}$ all transport terms vanish.
2. *Implicit Lagrangian phase* The pressure is iteratively refined
3. *Convective Flux phase* The transport term contributions are added

[1]The principle of virtual power corresponds to the principle of virtual displacements in solid mechanics

This scheme is not as limpid as the purely Lagrangian one and the second-order accuracy is only guaranteed for phase 1. Let analyze the whole scheme for further knowledge of the working procedure. The time integration can be described within the next 16 steps:

1. First compute $\underline{v}^{n+1/2} = \underline{v}^{n-1/2} + \Delta t \underline{a}_n$, where:

$$\underline{a}_n = \frac{\underline{F}_t^{old} + \underline{F}_p^n + \underline{F}_b^n + \underline{F}_s^n}{M} \tag{3.8}$$

$\underline{F}_t^{old}$ momentum transport forces at the end of previous step

$\underline{F}_p^n$ pressure forces $\underline{F}_b^n$ body forces $\underline{F}_s^n$ surface forces

2. Obtention of a new "Lagrangian configuration":

$$\underline{x}^L = \underline{x}^n + \Delta t \cdot \underline{v}^{n+1/2}$$

3. Evaluation of L-volume and L-density. This is possible because the mass M remains constant:

$$V^L = V^L\left(\underline{x}^L\right) \tag{3.9a}$$

$$\rho^L = \frac{M^n}{V^L} \tag{3.9b}$$

4. From the internal energy equation (3.6), the following is deduced without considering the transport term, and using the divergence theorem.

$$\frac{d}{dt}\left(\rho i V\right)) = -(p+q) \oint_S \underline{v} \bullet \underline{n} dS \tag{3.10}$$

Some pseudo-viscosity, q, is needed to stabilize the solution at shock fronts depending on the length of the element and dilatational wave speed

5. The former expression (3.10) can be approximated to the first order by:

$$\frac{(\rho i V)^L - (\rho i V)^n}{\Delta t} = -\left(p+q\right)^n \frac{V^L - V^n}{M^n} \tag{3.11}$$

6. Notice that $(\rho V)^L = (\rho V)^n = M^n$, so the internal energy can be consequently obtained as:

$$i^L = i^n - \left(p+q\right)^n \frac{V^L - V^n}{M^n} \tag{3.12}$$

7. i^L is just a first guess since the pressure changes over the step and it must satisfy as well the state equation.

8. Iteration of the following expression so as to obtain the L-value implicitly. Usually one or two iterations are sufficient.

$$p^l = f\left(\rho^L, i^L\right) \tag{3.13a}$$

$$i^L = i^n - \left(\frac{p^n + p^L}{2} + q^n\right)\frac{V^L - V^n}{M^n} \tag{3.13b}$$

9. Computation of the true end-of-step configuration:

$$\underline{x}^{n+1} = \underline{x}^n + \Delta t \cdot \underline{w}^{n+1/2} \tag{3.14}$$

10. Computation of the new volume V^{n+1}

11. The next step concerns the mass variation control. The mass transport across element boundaries must be accounted (face by face) so as to compute the new element mass:

$$M^{n+1} = M^n + \Delta t \cdot \oint_{S^n} \rho^L(\underline{w} - \underline{v})^{n+1/2} \bullet \underline{n} dS \tag{3.15}$$

12. For stabilization reasons, the density ρ_J (depending on the face J) is computed as a weighted average of neighbor elements' densities:

$$\rho_J = \frac{1}{2}\left[(1-\alpha_J)\rho^e + (1+\alpha_J)\rho^{e'}\right] \tag{3.16}$$

with,

$$\alpha_J = \alpha_0 \cdot \text{sign}(F) \qquad F = \Delta t \cdot \int_{S_J} (\underline{w} - \underline{v}) \bullet \underline{n} dS$$

$$0 < \alpha_0 < 1$$

$\alpha_0 = 0$: centered approximation. Problems with oscillations.
$\alpha_0 = 1$: full donor. It is too diffusive.

13. The new elements' density is obtained as:

$$\rho_e^{n+1} = \frac{M_e^{n+1}}{V_e^{n+1}} \tag{3.17}$$

14. Similar treatment then applied also to energy transport:

$$\frac{(Mi)^{n+1} - (Mi)^n}{\Delta t} = \left[\Sigma_J\left(\rho^L i^L\right)_J \int_{S_J} (\underline{w} - \underline{v})^{n+1/2} \cdot \underline{n} dS\right] + \frac{(Mi)^L - (Mi)^n}{\Delta t} \tag{3.18}$$

$$i^{n+1} = \frac{M^n}{M^{n+1}} i^L + \frac{\Delta t}{M^{n+1}} \left[\Sigma_J \left(\rho^L i^L \right)_J \int_{S_J} \left(\underline{w} - \underline{v} \right)^{n+1/2} \cdot \underline{n} dS \right] \tag{3.19}$$

15. The final pressure is get as:

$$p^{n+1} = f\left(\rho^{n+1}, i^{n+1} \right) \tag{3.20}$$

16. The nodal forces due to momentum transport (3.2) for the next step are:

$$F^e_{tiI} = \int_{V^e} N_I \rho^L \left(\underline{w} - \underline{v} \right)^{n+1/2} \cdot \underline{\nabla} v_i^{n+1/2} dV \tag{3.21}$$

3.3.2 Finite Volume Discretization

There are different ways of formulation in Finite Volumes. This section describes the Node-Centered Finite Volume formulation and the Cell-Centered Finite Volume formulation both used in the modeling of fluids.

Node-Centered Finite Volume (NCFV)

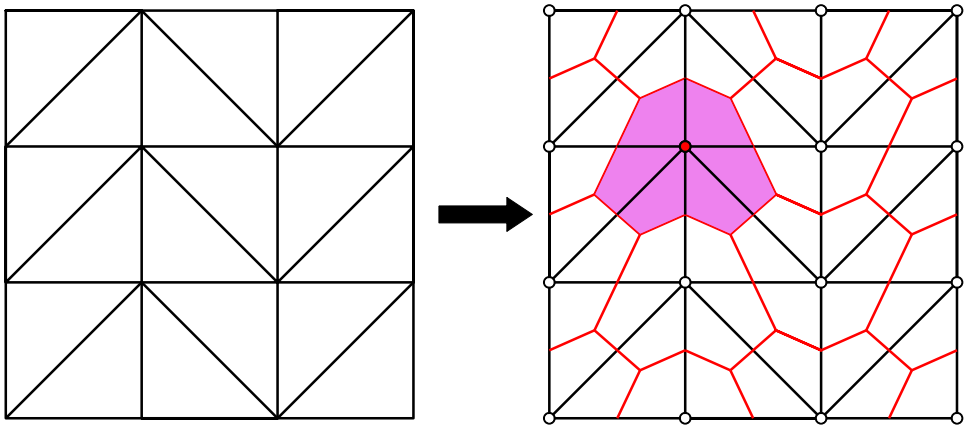

Figure 3.6: Node-centered FV fluid model.

The Euler Equations (3.1) (3.2) (3.3) are written in a conservative form with this formulation:

$$\frac{\partial \underline{U}}{\partial t} + \underline{\nabla} \cdot \underline{F} = \underline{0} \tag{3.22}$$

The weak form of the conservation equation is obtained by integrating them over a generic control volume V (fixed or moving in space) and by applying Green's (divergence) theorem:

$$\frac{d}{dt}\int_V \underline{U} dV = -\oint_S \underline{F}\cdot\underline{n} dS \tag{3.23a}$$

$$\frac{d}{dt}\int_V \underline{U} dV = -\int_{V(t)} \left[\frac{\partial \underline{U}}{\partial t} + \underline{\nabla}\cdot\underline{U w}\right] dV \tag{3.23b}$$

Using the Green's theorem in (3.23),

$$\frac{d}{dt}\int_V \underline{U} dV = -\int_{V(t)} \frac{\partial \underline{U}}{\partial t} dV + \oint_{S(t)} \underline{U}\left(\underline{w}\cdot\underline{n}\right) dS \tag{3.24}$$

The discrete conserved variables are integral means over the generic control volume V_I. It can be writen:

$$\underline{U}_I^n = \frac{1}{V_I^n}\int_{V_I^n} \underline{U}^n\left(\underline{x}, t^n\right) dV \tag{3.25}$$

The above equations are integrated in time over an interval $\Delta t^n = t^{n+1} - t^n$ and , after some further manipulations, the following general scheme is obtained:

$$V_I^{n+1}\underline{U}_I^{n+1} = V_I^n \underline{U}_I^n + \Delta t^n \underline{\Phi}_I^* \tag{3.26}$$

Where,

$$\underline{\Phi}_I^* = \Sigma_{J\in\Psi(I)} N_{IJ}\left(\underline{U}_{IJ}^* w_{IJn} - \underline{\varphi}_{IJ}^*\right) \quad \text{(assembled numerical fluxes)}$$

$$(\varphi_k^*)_{IJ} = (\underline{F}_k^*)_{IJ}\cdot\underline{n}_{IJ}^* \quad \text{(flux matrix projection)}$$

The calculation of numerical fluxes is done by using Roe's approximate Riemann solver [9] for the Riemann problem defined by each couple of neighboring volumes' physical states.

The solution is advanced in time by explicit "first-order" scheme presented above (3.26), irrespective of the desired accuracy. The obtained accuracy in space and time of the update depends only on the procedure used to compute the numerical fluxes $\underline{\Phi}_I^*$:

- Choosing $t^* = t^n$ and node-centred values in space gives first-order accuracy in time and in space.
- Choosing $t^* = t^{n+1/2}$ and spatially extrapolated intra-cell boundary values gives second-order accuracy in time and in space[2].

[2]To obtain second-order accuracy in time and in space, van Leer's MUSCL-like technique is adopted. It combines a predictor-corrector scheme in time with a spatial extrapolation of the conserved variables to

Nevertheless, to make FE and NCFV formulations compatible, in view of performing FSI simulations by Lagrange multipliers, the two schemes must be properly synchronized.

The NCFV peculiarities have been gathered and summarized in the next list:

- All quantities of velocities and pressures are discretized at nodes.
- Physical status of FV depends only upon its volume, not on its shape. As it is known fluids adopt the shape of their enclosure, so this is OK for them. However, geometry is still used to compute volume and fluxes.
- The transport is computed internally to each FE (figure 3.7), there is no need to know neighbor FEs.

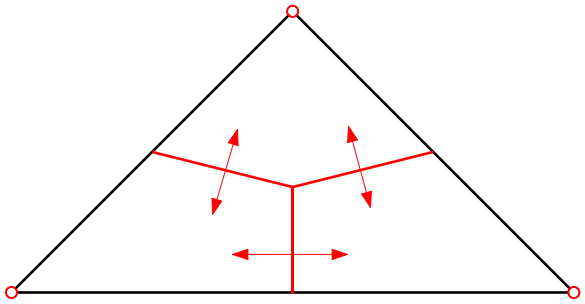

Figure 3.7: Transport among FV.

- Equivalence between FE and NCFV concerning the initial conditions is not straightforward as seen in the figure 3.8.

  As the limits are not the same, the boundary conditions can not have the same meaning in both problems because of the discretization. Some possible remedies are the ones shown in the figure 3.9. The idea is to play with the geometry in order to balance the information in both regions and construct a kind of "average" BC border.

Cell-Centered Finite Volume (CCFV)

Cell-Centered Finite Volume formulation is developing right now. Recent researches suggest that CCFV will be the formulation of the future (the references [10] and [11] are some examples of the undergoing research).

As shown in the figure 3.10, here you have CCFV's particularities:

- FV mesh coincides with the classical FE mesh.

intra-cell boundaries.

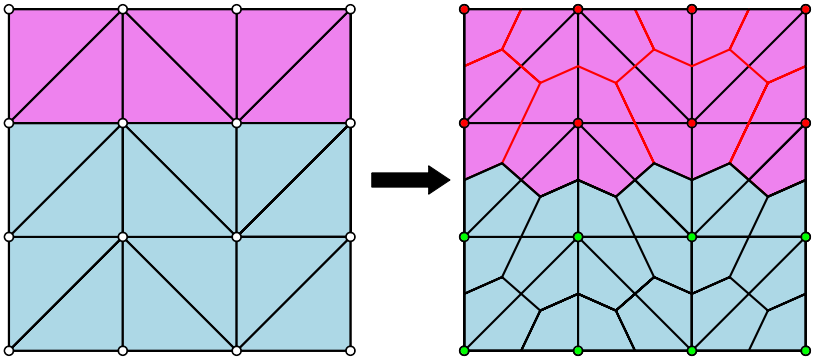

Figure 3.8: Application of boundary condition.

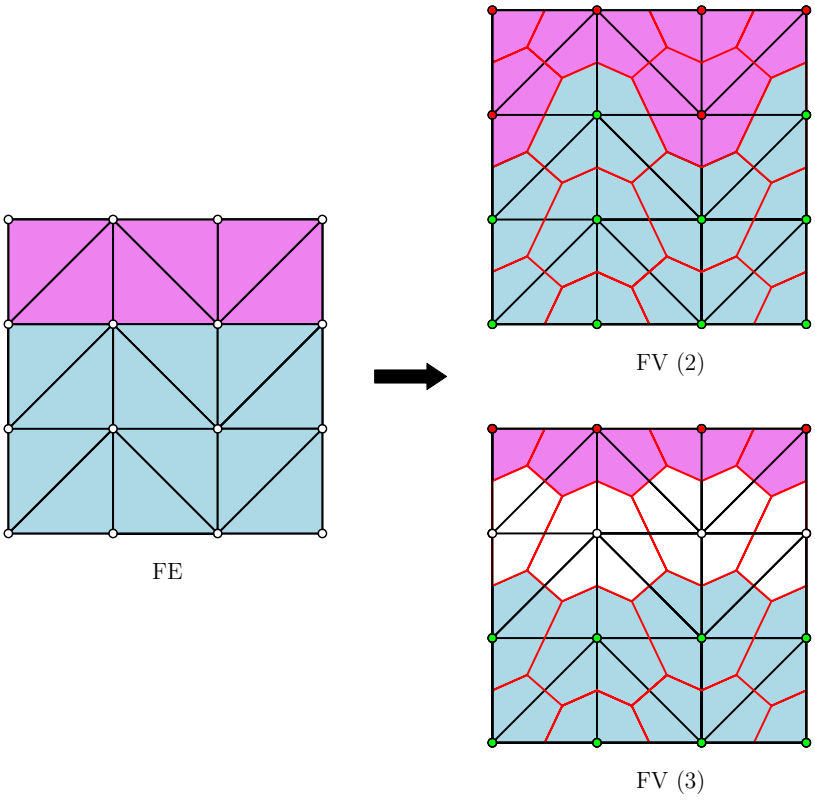

Figure 3.9: Possible remedies and strategies for BC's treatment.

- All quantities are discretized at "cell" centers in the FV discretization.
- Initial conditions are set like in FE.

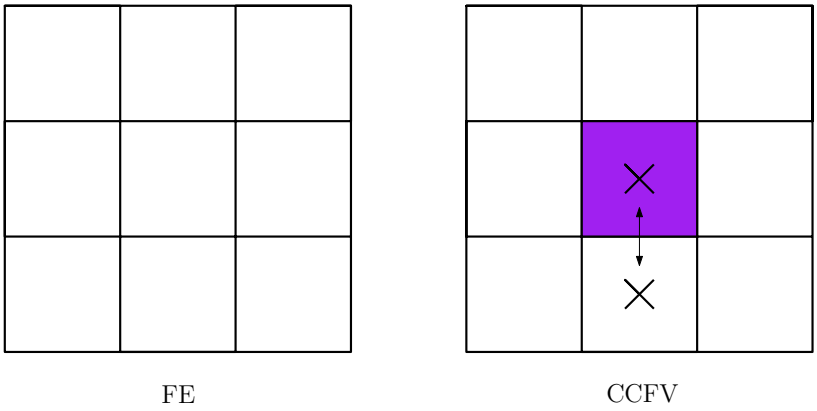

Figure 3.10: Mesh generated from the FE.

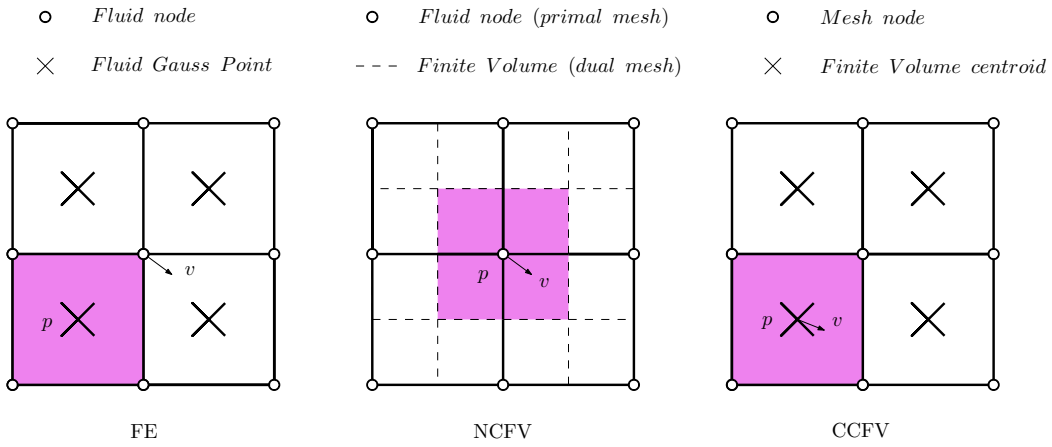

Figure 3.11: Graphical comparison between FE, NCFV and CCFV.

3.3.3 Mesh Rezoning Algorithms

Rezoning is necessary in ALE formulation because Lagrangian solutions suffer from excessive distortions and entanglement. Lagrangian formulation attach the particles to a certain space in their mesh, so huge changes of volume can not be properly represented by this formulation.

The figure 3.12 represents the behavior of an explosion inside a reactor vessel. Once the explosive bubble is detonated, the lagrangian mesh follows the material. This distortions the reality as bigger elements have to be computed due to the sudden expansion of the pressure. On the contrary, this does not the case of the rezoning system in the figure 3.13, and the reality is much better simulated in this second approach.

Rezoning means a motion of nodes belonging to an ALE mesh at constant mesh topology. Do not confuse rezoning with remeshing or adaptivity. There are different types of rezoning:

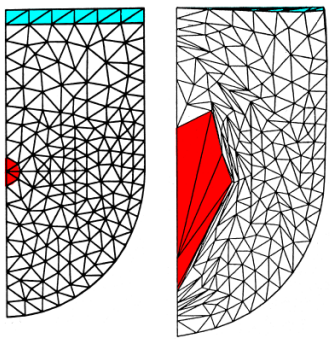

Figure 3.12: Lagrangian triangles discretization, see [2].

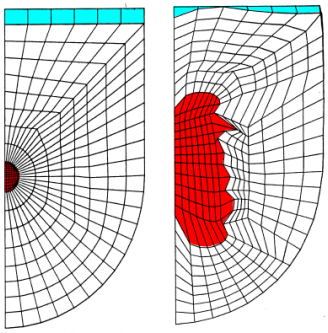

Figure 3.13: ALE manual rezoning with quadrangles, see [2].

Kinematic "Slave" nodes follow the "master" nodes. The slave nodes are defined along a line by master end-points. In case of nodes inside a triangle, quadrangle, etc. slave nodes move homeomorphically

Geometric There are various ways included in the *geometric rezoning*. This document analyzes mean value algorithms and the Giuliani's method [12], which minimizes triangles/tetrahedra distortion.

Mechanic The elasticity equations are solved for a dual mesh (ALE grid) considered as a solid (continuum, bar assembly, etc.). Explicit formulation is used to save CPU.

Mean-based Algorithms

The idea behind the mean-based algorithm is very simple: the optimal position of a node is the mean of its neighbors. Alternatively the use of displacement instead of position is sometimes used.

$$\underline{x}_I^r = \frac{1}{n}\Sigma_{P=1}^{n}\underline{x}_P \tag{3.27}$$

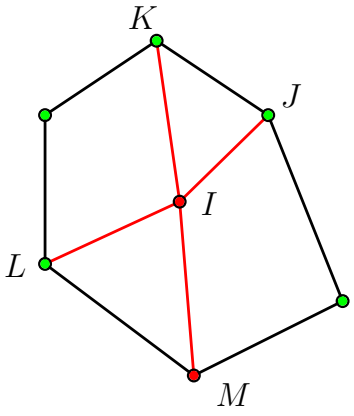

Figure 3.14: Graphic illustration of mean-based node positioning.

Experience has demonstrated that there are some drawbacks. Mean-based rezoning algorithms rapidly tend to produce uniform meshes, which can be unwanted in some cases. In addition, some special configurations seem to be impossible to rezone with this procedure (local mesh curvature).

Giuliani's algorithm

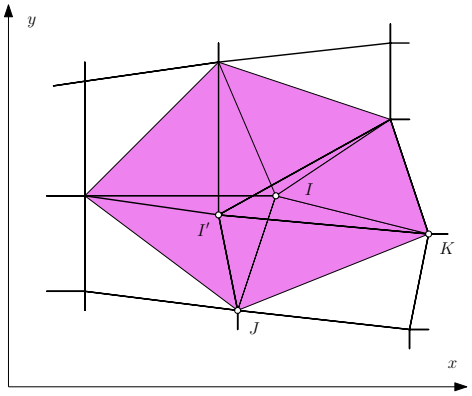

Figure 3.15: Giuliani's automatic rezoning influence domain.

Giuliani's algorithm identifies for each ALE node an influence domain made of neighbor triangles (figure 3.15) or tetrahedra in 3D. Once the domain has been built, the "shear" and "stretch" is measure in each measure in the domain (figure 3.16).

$$\text{shear} = f(d)$$

$$\text{stretch} = g(h)$$

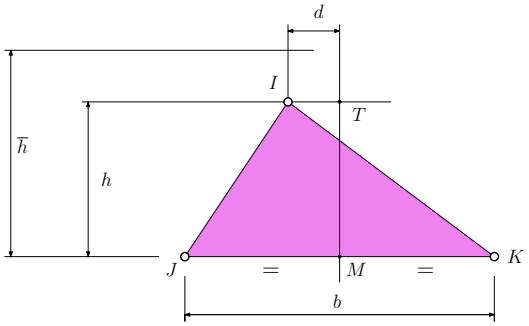

Figure 3.16: "Shear" and "stretch" measurement.

$\overline{h}$ is the mean height of triangles in the influence domain

The objective turns to minimize a function of total shear and stretch over the node's influence domain, with special care for nodes subjected to boundary conditions:

$$E = \sum_{i=1}^{N} \left(\frac{h_i - \overline{h}}{\overline{h}} \right)^2 + \sum_{i=1}^{N} \left(\frac{2d_i}{\overline{b}} \right)^2$$

$$objective = min\{E\} \tag{3.28}$$

Chapter 4

Fluid-Structure Interaction

4.1 Motivation and Classification

For years problems concerning a system formed by fluid and structure have been modelized separately. This uncoupled approach computes the fluid first and in a second calculation it takes the pressures from the fluid so as to deal with the structural problem.

The other approach is to treat the system as fully coupled, taking into account the interaction of both, the fluid and the structure.

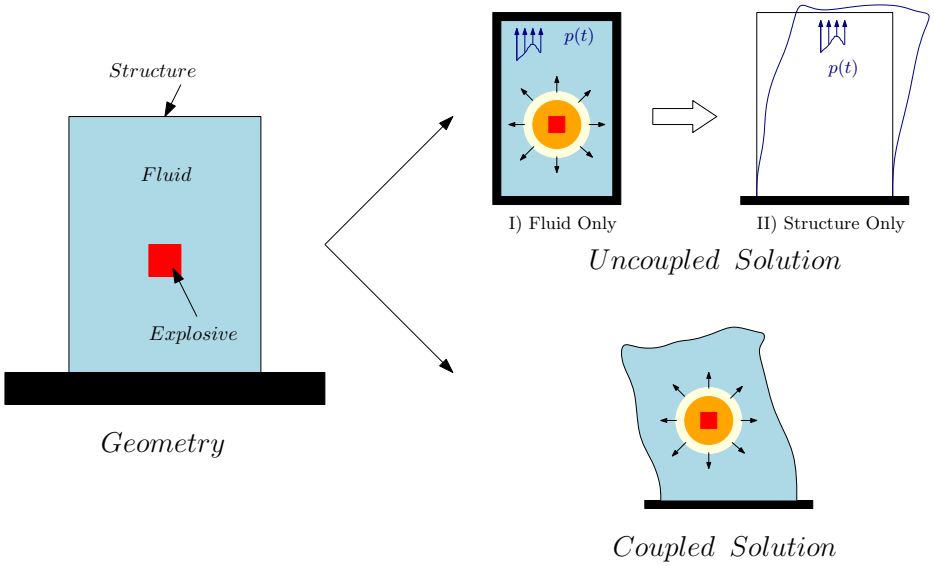

Figure 4.1: Two possible approaches.

But, fully coupled analysis is sometimes mandatory, specially in two classes of problems:

- With nearly incompressible fluids
- With very deformable structures

There are plenty of FSI algorithms available in the literature, but all of them must solve two main problems: *the geometrical mesh matching* and *the mechanical coupling*. The first one deal with the relation between the nodes of the structure and the fluid domain, whereas the second threats the coupling and the motion transmission of both components. The figure (4.1) gathers all the options that the code offers to deal with FSI problems. This is the general vision one should have in mind concerning FSI problems.

Geometrical Mesh-Matching	Mechanical Coupling
Failure	Strong
	Weak
Non-Failure	Strong
	Weak

Table 4.1: General overview of the FSI approaches

This chapter 4 describes and explains the main approaches to simulate *fluid structure interaction*.

4.2 Geometrical mesh-matching

Once having the determination to solve a fluid-structure problem in an coupled approach there are some points to take into account from the very beginning. The correct discretization of the domain is vital. Not only to run certain code, but also to get results as accurate as possible. The final output will be consequence of how attentive the user is concerning the mesh generation. So, the first step is to understand the whole system and the final objective in order to build the correct work-strategy; if not, the results will be completely random.

The mesh generation is closely related with the structure's response to the external loads. The approach will be different in terms of geometry, if the assumption of structural failure is done or not. For non structural failure, an intuitive and basic mesh construction is hold. To compute failure in the structure, an embedded mesh is the correct election.

Notice the different meaning of *failure* depending on the context. Here, failure describes a "broken"solid structure, divided into debris which no longer suffers from external loads. Remember that the interaction of the fluid and structure is happening in a very short time, for very huge loads, so the structures may easily suffer from fragmentation. Structural failure refers to the moment once this fragmentation have taken place, allowing flow though the damaged structure.

4.2.1 Isolated fluid cells

Non Structural Failure hypothesis means that the structure and the fluid will be permanently in touch, and the fluid cells isolated. The fluid will never come through the structure, and two fluids separated by a solid structure will never be in contact. This intuitive idea marks the way the mesh should be drawn.

As the fluid and the structure are immiscible, they can not share the same nodes in the general mesh. That is why generally both the structure and the fluid are discretizated separately. The user have to ensure that the interface between fluid and structure is double and formed by fluid nodes and structure nodes.

Nodal conformity

This spatial discretization could be different depending on the element's size of the components. If the nodes in the interface are located in the same spatial point the mesh is called *conforming*. On the contrary, if the same refinement for both is not needed and the nodes are not longer doubled in the interface, the mesh is called *non-conforming* (figure 4.2).

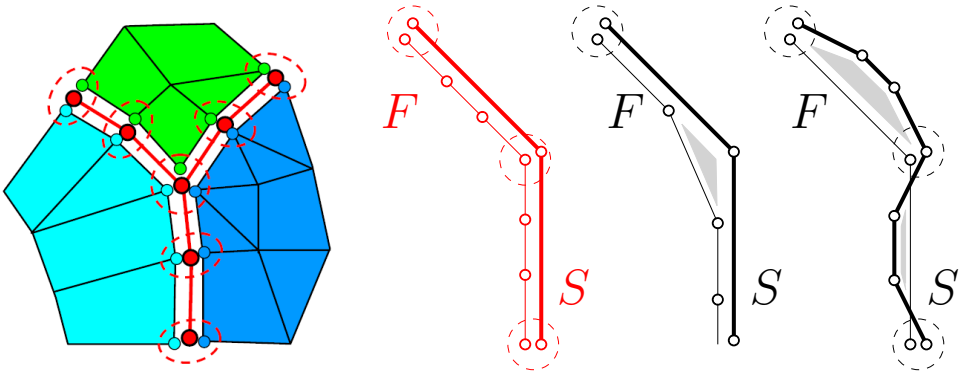

(a) Conforming mesh (b) Non-conforming mesh

Figure 4.2: Conformity and Non-Conformity in meshes.

The conformity is widely used and its application is justified in almost the majority of practical applications, because of the following reasons:

- Linear-velocity, uniform-pressure elements are used for the fluid.
- Zero-thickness shells are linearly interpolated along membrane.
- External pressure on shells element-wise uniform
- An the most important one, because this conforming technique ensures the maximum simplicity and optimal accuracy.

However, the conformity requirement can be removed to obtain an even more general treatment of permanent FSI, which can be very useful in specific advanced applications. In fluid analysis for instance, small elements are needed and it is not necessary to discretize the structural domain with the same length of element. So, non-conformity allows the user to save computer memory and calculation time.

The figure 4.2 b) shows a tentative classification of non-conforming meshes. But is the first which seems to be the most attractive in practical applications; normally, the fluid domain is refined more than the structure. The so-called *hierarchic configuration* works properly, since for a given mesh size, the stability step is usually larger in fluid elements than in structure, and it produces no gaps/overlaps.

4.2.2 Flow transference through damaged structure

The structural failure will lead to its erosion and this must be somehow treated (figure (4.3)). The basic mesh construction described above are no longer applicable in this case as the failure would mean that two separated fluids might share nodes, and this continuity is simple impossible by definition. In addition, there are other reasons that make incompatible structural failure with the model described above in 4.2.1:

- Difficult to sew the fluid meshes on either side of the failing structure
- Automatic fluid mesh rezoning algorithms fail because the master domain (structure) "disappears"
- Possible rotating macro fragments create rezoning problems.
- Etc.

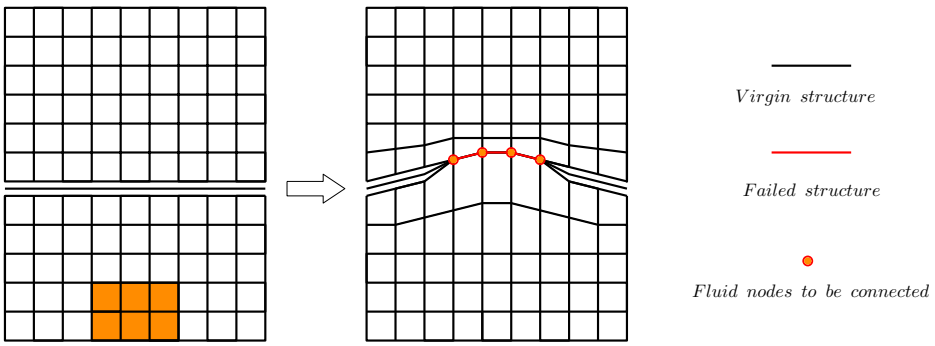

Figure 4.3: FSI mesh treatment after failure.

This is an alternative in order to deal with failure and fragmentation problems. It decouples structure from fluid from the initial discretization as shown in the figure 7.1. The

structure is inside an external fluid mesh, which simplifies the mesh generation, as the user could be unaware of any matching or non-matching structure and fluid nodes.

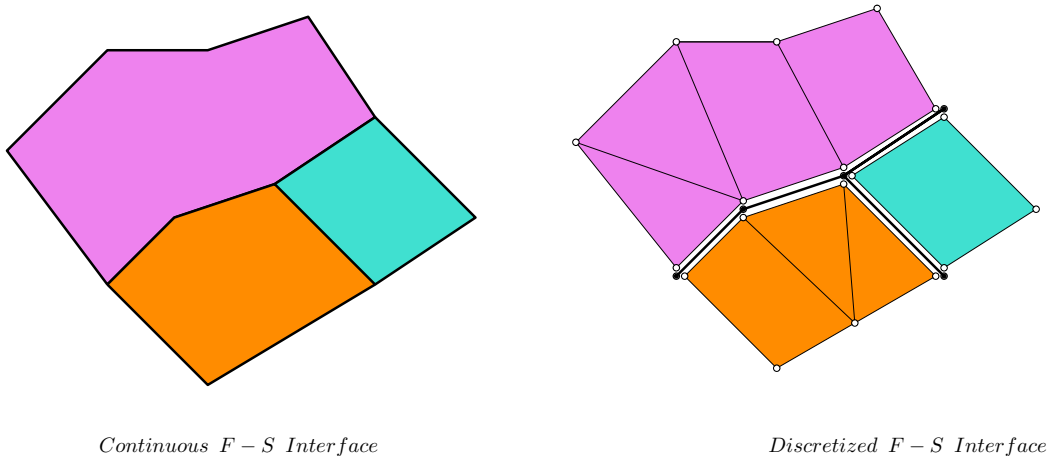

(a) Fluid-Structure Interaction

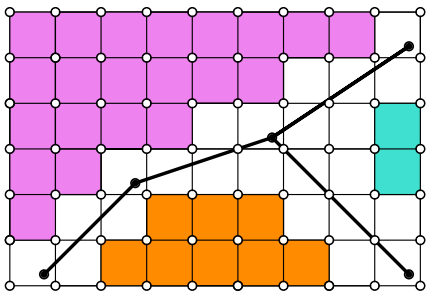

(b) Alternative embedded mesh

Figure 4.4: Alternative methodology

The fluid mesh can be structured, eulerian and with no entanglements for large rotations by construction. The structure is discretized independently from the fluid and its mesh is embedded or immersed in the fluid mesh. On the other hand, there are a few drawbacks. A higher numerical diffusion is expected in comparison with the the basic mesh construction for non-failed analysis, so in general less accuracy is obtained. That's why locally a finer mesh is required.

4.3 Mechanical coupling

Once the mesh is geometrically well constructed, the following step is to define the *mechanical coupling strategy*. This means the definition of the interaction of the fluid and structure, which is directly linked with the type of enforcement desired and the finite element or finite

volume elected in the discretization.

In most of the cases the structure is the external boundary of the fluid, and the fluid's behavior defines the boundary conditions for the structure. The way this interaction occurs is the *mechanical coupling*. This FSI enforcement might be classified in two groups, depending on the type of the constraint imposed in the interface. The followings:

Strong mechanical coupling Via constraints on velocities. Constraints on Fluid and Structure velocities are imposed by lagrange multipliers (implicit).

Weak mechanical coupling Via pressure forces and fluxes. Pressure forces are transmitted from the fluid to the structure and structure motion provides weak feedback on fluid.

4.3.1 Strong coupling

Strong coupling is related with the treatment of the nodal velocity in the interface. As shown previously, the surface contact must be modelized, and it seems that an ALE formulation fits normally. The problem can be easily turned decoupled by introducing a constant pressure along the surface (figure 4.5). For an inviscid fluid the pressure acts along the normal $\underline{n}$ to the interface.

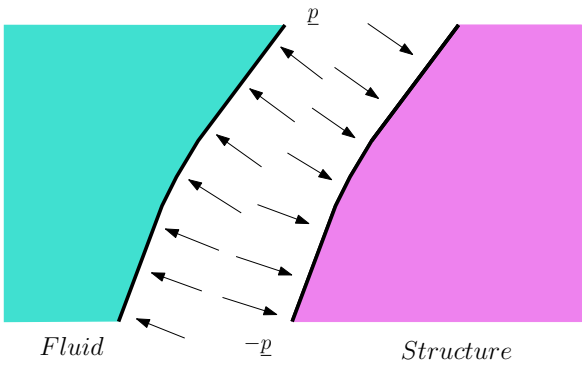

Figure 4.5: Decoupled problem.

Then, the material velocity compatibility condition should be imposed, in other words, the strong coupling conditions or the velocity constraints:

$$\underline{v}_F \bullet \underline{n} = \underline{v}_S \bullet \underline{n} \tag{4.1}$$

- Tangential velocity components are unconstrained
- Mesh velocities at interfaces obey $\underline{w}_F = \underline{w}_S$

Upon discretization, contact pressure is replaced by interaction force $\underline{r}$. This interaction force $\underline{r}$ is the resultant of the contact pressure at each node of the interface (figure 4.6), using nodal conformity at the F-S interface. Velocity capability condition (4.1) is of the form $\underline{\underline{C}}\underline{v} = \underline{b}$ (2.25), therefore Lagrange multipliers (2.27) can be used to find $\underline{r}$.

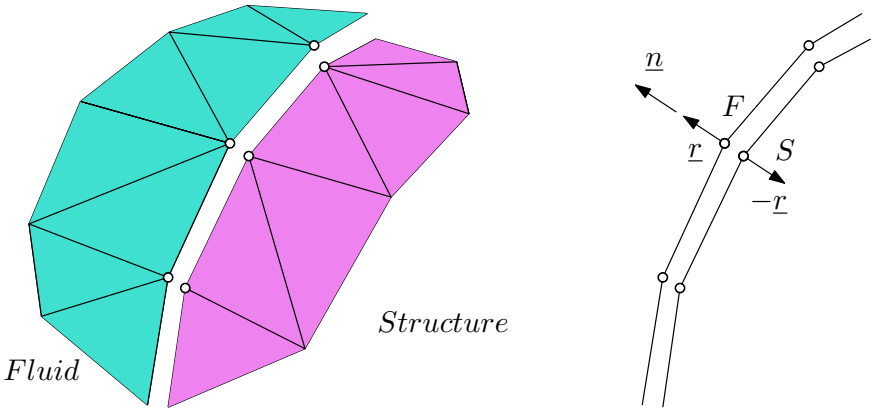

Figure 4.6: Interaction force in each node.

However, simple questions arise from this explanations: how is defined the normal to a discrete F-S interface? Not only F-S interfaces, but also geometrically more complex cases, such as bilateral fluid contact, structural joints, submerged structural edges or structural elements without topological thickness. What is more, for the explanations above conformity has been supposed, but that is not mandatory as it has been explained previously.

The generalization of coupling (velocity compatibility) conditions for non-matching, where $\underline{n}_F$ is the normal to the fluid domain is described in the equation (4.2) and shown in the figure 4.7 .

$$\underline{v}_F \bullet \underline{n}_F = \underline{v}_{S^*} \bullet \underline{n}_F = \left(c_1 \underline{v}_{S_1} + c_2 \underline{v}_{S_2}\right) \bullet \underline{n}_F \tag{4.2a}$$

$$\underline{w}_F = \underline{w}_{S^*} = c_1 \underline{w}_{S_1} + c_2 \underline{w}_{S_2} \tag{4.2b}$$

And last but not least, the hypothesis of failure or non-failure might have different mechanical coupling treatment. The interface non-conforming geometrical mesh matching or a failure-type material election will determine further mechanical coupling conditions, so those are a factors to take into account.

There are plenty of options that this document will not analyze as it is not the objective. Nevertheless, some of the methods used in the examples have further explanations and descriptions in this section.

Geometrical FSA/FSR method

The FSA algorithm [13] is a mechanical strong coupling method, based upon local shape

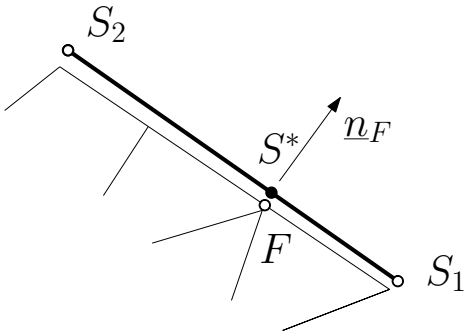

Figure 4.7: Non-matching node.

of fluid domain only and valid for non-failure treatment. This method computes the normal vector of a surface, in a purely geometrical way.

The normal direction ($\underline{\Delta}$ = influence domain of the node) is obtained from zero net velocity flux condition across discrete interface where no fluid is gained or lost (figure 4.8):

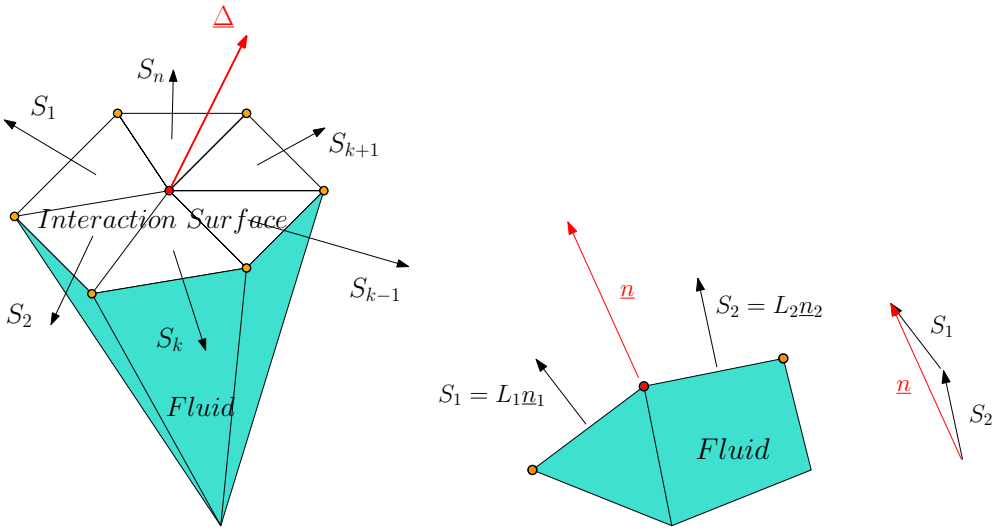

(a) 3D (b) 2D

Figure 4.8: FSA normal computation.

With no lost of generality the normal is calculated using the following formula, for 2D and 3D:

$$\underline{n} = \underline{\Delta}/\|\underline{\Delta}\| \quad \text{with} \quad \underline{\Delta} = \sum_{k=1}^{n} \underline{S}_k$$

($\underline{\Delta}$ = influence domain of the node)

The face vectors, $\underline{S}_k$, are subdivided into one or more groups, and each group is used to generate one normal. Vectors pertain to a specific group if they form a smaller angle than a given $\overline{\gamma}$. If the number of independent normals equals the space dimension, the node is set Lagrangian and "tied" to the structural node which means that $\underline{v}_F = \underline{v}_S$.

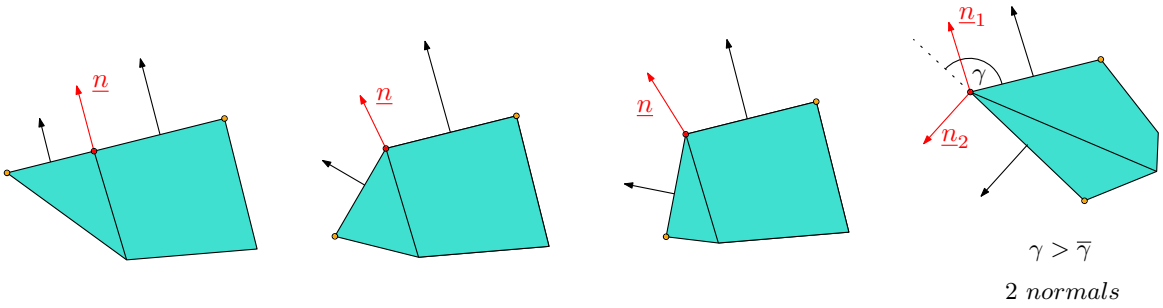

Figure 4.9: Effect of progressive "sharpening" of interface corner. Different normals depending on the angle between faces.

Expanding what it has been explained, in 3D cases, there might be 1 or 2 normals in an ALE node. In the figure 4.10, 3 points are highlighted: A, B and C. A has 1 blocked normal and 2 free directions; B has 2 blocked movements and only 1 free direction; whereas the point C has every movement direction blocked. This last point is fixed so $\underline{v} = 0$, and by definition it behaves as a Lagrangian point in the space.

FSA method is purely geometrical and uses no information about internal fluid element formulation, so slight but non-negligible accuracy mismatch in calculation of internal pressure forces and of the reactions, may create onset of spurious velocities in 3-D models with warped element faces (the patch test is a common example in the literature, where a rigid box filled with uniform pressure is modelized). This leads to a further investigation in alternative methods based on equilibrium.

In the case of rigid structures the Fluid Structure Rigid (FSR) method is used. An structure is treated as rigid when its displacements are known to be negligible. In those cases only the fluid needs to be modelized.

The computation turns much more easy as the normal, $\underline{n}$, remains constant in time and the compatibility condition simplifies to $\underline{v}_F \bullet \underline{n} = 0$. The geometric and equilibrium methods can be used unchanged, apart from suitable simplifications that the structure's rigid condition offers. In practice, the automatic FS directives dramatically simplifies the prescription of boundary conditions in geometrically complex cases.

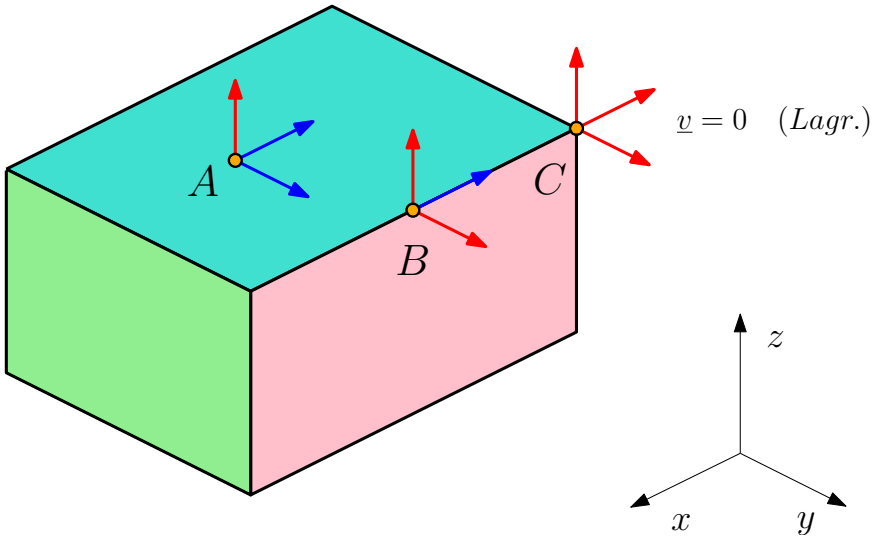

Figure 4.10: ALE node behavior in 3D formulation.

Equilibrium-Based methods. Uniform Pressure method

The method simply relies upon the observation that the direction of the discrete normal coincides with the resultant of internal forces due to an arbitrary but uniform pressure (say, $p = 1$) in the whole fluid domain. This is, as well as the FSA and FSR, a mechanical strong coupling method to compute the normal vector, but a non-geometrical one. The Uniform Pressure method is based upon equilibrium considerations. The meaning of this idea is well described in the figure (4.11):

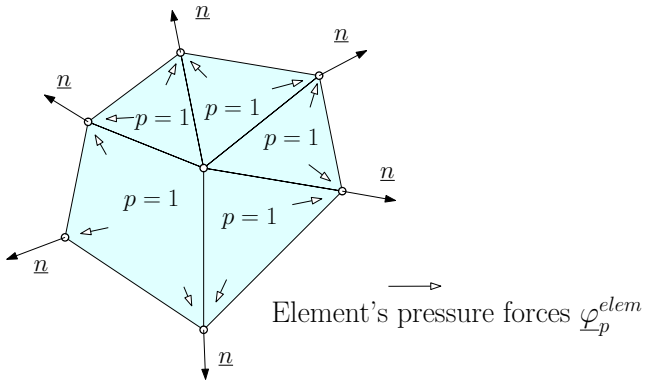

Figure 4.11: Arbitrary and uniform pressure in the domain.

The normal is computed as:

$$\underline{\varphi}_p^{elem} = \frac{1}{p}\underline{f}_p^{elem} \quad \text{Assembly} \quad \underline{n} = \underline{\varphi}_p / \|\underline{\varphi}_p\|$$

Its main advantages are that it is computationally inexpensive because $\underline{f}_p^{elem}$ are computed anyway. UP ensures perfect equilibrium, and therefore avoids shortcomings of purely geometrical methods, such as FSA with warped 3-D faces.

On the other hand, there are also some shortcomings in the UP algorithm. It fails at submerged structural edges, with no topological thickness, because the assembled force vanishes each other and thus the normal is undetermined. In addition, it can yield at most one normal per node, and as it has been shown before there are some cases where blocking more than one movement is necessary.

Combined method. FSCR method

The FSCR method is a combination of FSA and UP, exploiting their respective strengths. The algorithm searches for the best normal computation, whether by FSA $\underline{n}_1$ and $\underline{n}_2$ or by UP $\underline{n}_p$. That is why it is so-called an Hybrid method.

There are mainly two options:

1. If FSA yields influence domain composed only by mutually opposite faces, $\underline{n}_p$ is undetermined. In this case $\underline{n}_1$ and $\underline{n}_2$) must be kept.
2. In all other cases $\underline{n}_p$ is more accurate than $\underline{n}_1$ and $\underline{n}_2$. If there is only one FSA normal $\underline{n}_1$, we take $\underline{n}_p$ instead. Else, if there are two FSA normals, $\underline{n}_1$ and $\underline{n}_2$, the normal is corrected so that $\underline{n}_p$ is contained in the plane defined by $\underline{n}_1^{'}$ and $\underline{n}_2^{'}$ (figure (4.12).

FLSR method

The FLSR method is a way of computing embedded models. This section describes how it works and gives some characteristics.

For embedded meshes first an "influence domain" must be built up around the structure so as to identify the fluid nodes currently located within the influence domain of the structure as seen in chapter 4.2.2 . Then, one must impose suitable constraints on velocity (4.1) matching the fluid node with the closest structural node. Each coupling condition involves one fluid node. Notice that the velocities constraints for the structure are not computed in nodes in general, but in points S^* (4.3)

$$\underline{v}_F \cdot \underline{n} - \underline{v}_{S^*} \cdot \underline{n} = 0 \tag{4.3}$$

The fluid mesh can be structured, eulerian and with no entanglements for large rotations by construction. The structure is discretized independently from the fluid and its mesh is embedded or immersed in the fluid mesh. On the other hand, there are a few drawbacks. A higher numerical diffusion is expected in comparison with the FSA method, so in general less

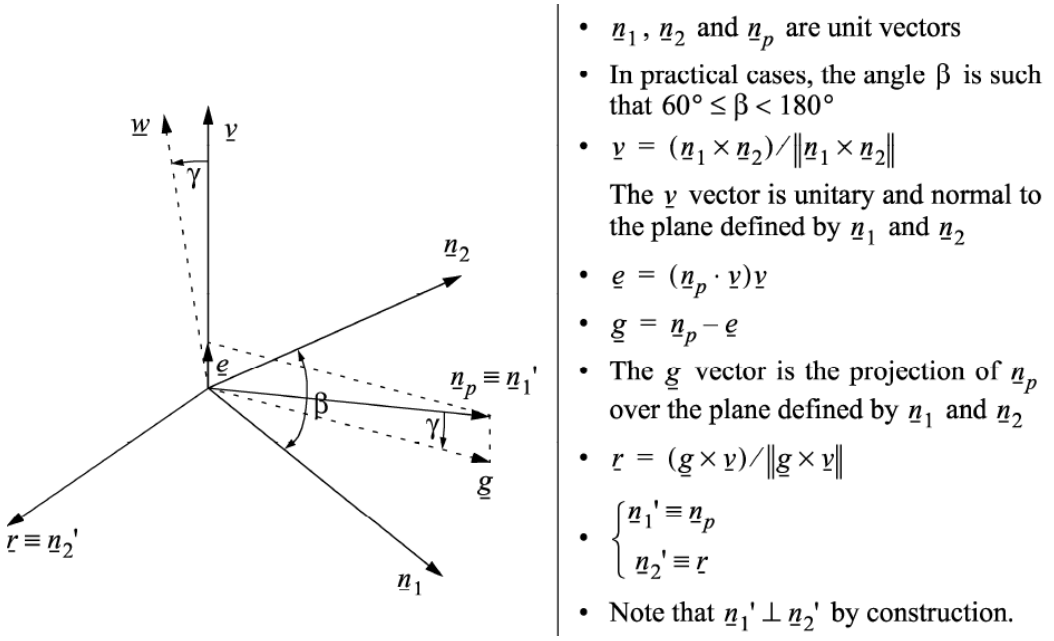

Figure 4.12: Correction for n_p when FSA computes both n_1 and n_2, see [2]

accuracy is obtained. That's why locally a finer mesh is required. Besides, as the influence domain is the union of various entities, suitable precedence rules are needed to when a fluid node belongs to more than one entity.

Influence of the element in weak coupling

The methods described above in a FE context have been applied successfully to Node-Centered Finite Volumes.

Nevertheless some adjustments are needed, since FV time integration scheme is Forward Euler and not CD (as for FE). The two schemes can be reconciled by adding a suitable force term to the equilibrium equation (2.6).

Velocity constraint on $\underline{v}_I$ can appear "too strong" since the boundary node I represents the average of the whole volume as shows the figure 4.13. In fact, the Fluid and the Structure are "strongly linked" together by the imposed constraints on velocities at F-S interface.

4.3.2 Weak coupling

There exists another technique called *weak coupling*. In this mechanic enforcement technique, suitable fluid pressure forces are introduced and transmitted to the structure. The structure then determines the motion of the F-S interface, and this provides a "weak" feedback on the physical status of the fluid, via interface velocity. This technique is nowadays

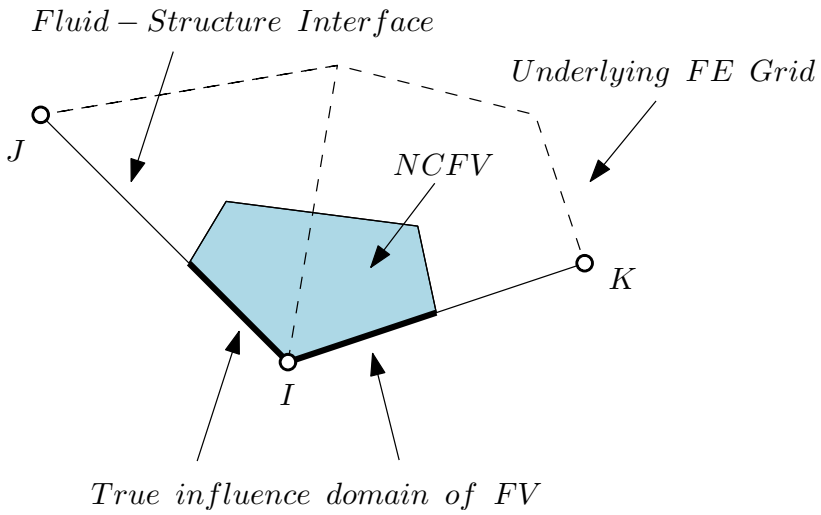

Figure 4.13: NCFV representation and its influence domain.

available for Cell-Centered Finite Volumes and for failure and non-failure material type.

First of all, it must be remembered that in Cell-Centered Finite Volume fluid velocities, pressure etc. are defined at the volume centers and not at nodes. This particularity led to its successfulness computing certain FSI problems.

Fluxes are not computed towards the boundary, as volume faces delimited the interface between fluid and structure. Therefore, zero normal velocity condition is "automatically" satisfied in an approximate way at a rigid wall. Also at cell centres, in a weak manner. If a structure is attached (merged nodes) to the fluid boundary, the code automatically computes pressure forces and applies them to the structure ("weak" FSI coupling). No flux calculation takes place at the boundary since volumes on the interface have no neighbors: a rigid-wall condition results automatically.

CCFV provides the possibility to merge fluid and structure nodes. This might be helpful apart from the mesh construction, to represent deformable structural boundaries (no need of FSA conditions) or in case of "double" FS Interface.

A non conforming treatment can be also compute with CCFV. In those cases, cell-centered fluid pressures are applied to the structure as shown below in figure 4.15, as long as the structure is not failed. Fluxes are not computed across a neighboring (unfailed) structure. Matching nodes can be irrelevantly merged or not, although the code used in the examples needs the non-matched nodes to be declared in a list.

But if the structural failure has to take into account CCFV may also be used in embedded FSI algorithms. The FLSW method is an example of it.

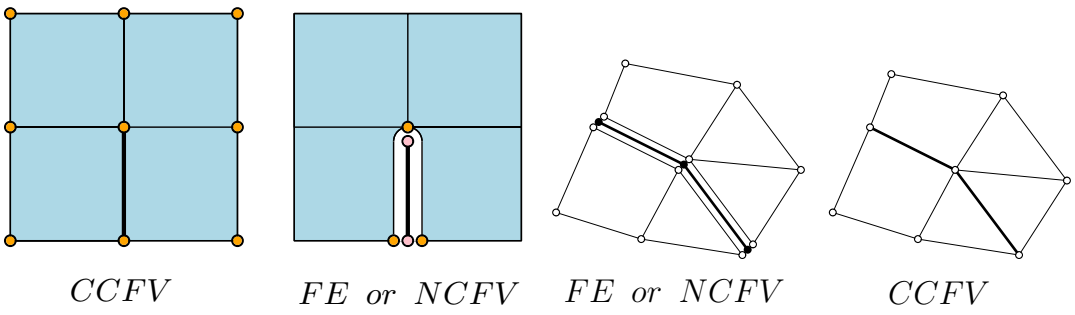

(a) Deformable structures (b) Double FS Interface

Figure 4.14: Merged structure and fluid nodes.

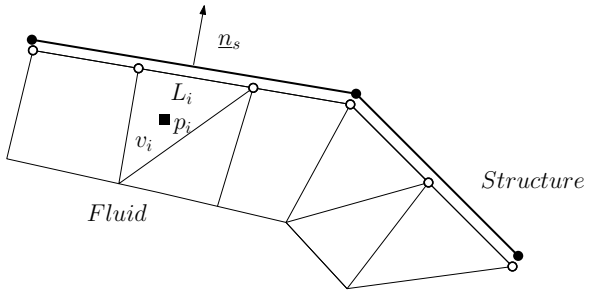

(a) Discretization

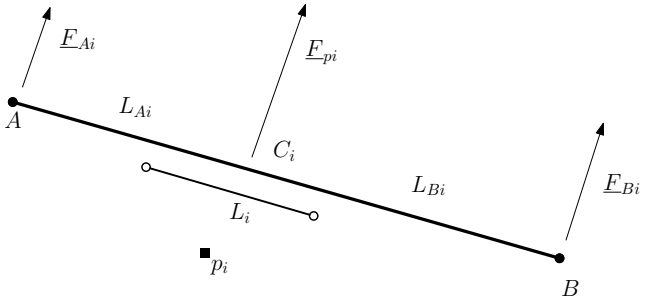

(b) Applied Forces

Figure 4.15: Cell-Centered fluid pressures' application.

FLSW method

The FLSW is a "weak" variant of FLSR to use with CCFV. As for FLSR first the "influence domain" must be defined around the structure. Then, fluid volume centers or fluid faces currently located within the influence domain must be identified with a fast search. There are 2 strategies to do it (see figures 4.16 and 4.17). Finally, pressure drop forces must

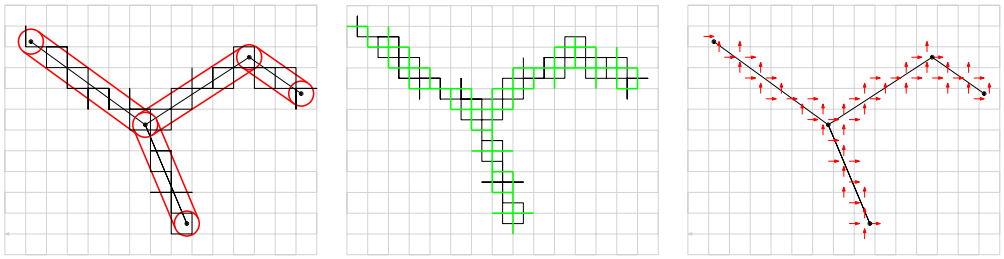

(a) Influence domain and associated FV faces

(b) Blocked fluxes

(c) Forces to be applied to the structure

Figure 4.16: Strategy A. Detect directly fluid faces

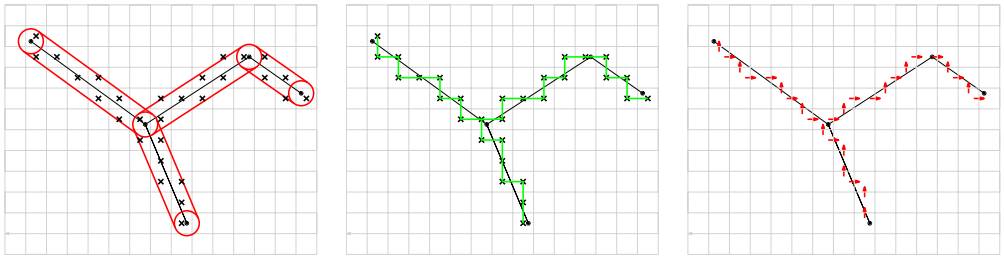

(a) Influence domain and associated FV faces

(b) Blocked fluxes

(c) Forces to be applied to the structure

Figure 4.17: Strategy B. Detect fluid elements, then faces

be transmitted to the structure and the associated mass and energy fluxes blocked. As in NCFV for FLSR method, it is necessary to block the numerical fluxes in FLSW calculation.

Chapter 5

Building Vulnerability

5.1 Motivation

The Fast Transient Dynamic Phenomena has been closely related with terrorist attacks, and therefore, great commissions and research groups are developing simulation software in order to prevent the feedback of those actions, and minimize as much as possible the hazards. Further designs improvements are already done, and some of them are compulsory in our nowadays' architecture.

Figure 5.1: New York Times 11-S. Source: NYT

This is also the case of the EUROPLEXUS code, that has been developed jointly by JRC an CEA and distributed by Samtech S.A.

5.2 Approaches to simulate an explosion

Depending on the characteristics of the explosion, there are different approaches to model it. On the one hand is up to the user to specify the analysis of the domain, taking into account the structure's motion, or even simplifying the problem without modeling the fluid domain.

On the other hand, there are several approaches to define the explosion, and a decision has to be made on that issue. This section describes the different ways to simulate an explosive charge.

5.2.1 Domain modeling

There are mainly three approaches to simulate an explosion: defining only the structure, simulating the behavior of the fluid for a rigid structure, and attaching the fluid-structure interaction.

Modeling only the structure is computationally cheap, but it has also its drawbacks. The effects of the detonation have to be somehow transmitted to the structure's boundary. This is achieved through an empirical formulation in function of distance and time between the location of the charge and the pressure's application point (figure 5.2). Obviously the user does not get the whole information, as reflections and completely shadow faces are not well computed in this way. It is commonly used because of its advantages in terms of computer economy and for a first approach.

On the other hand, the fluid can also be treated without taking into account the structure. This is only valid for very heavy and stiff structures, where they can be considered as completely static. The worst drawback is that the output does not specify the structural damage, so it is not a good approach to analyze building vulnerability. Nevertheless it is useful to study the pressure's evolution in the air, so as to know where the maximum and minimum points are.

And last, both the structure and the fluid may be modeled and the interaction studied. This allows the analysis of both at the same time, so the results are much more real. It is the unique way to treat the system as coupled, to define reliable risks maps, and structural damage figures. All effects are included in this type of computation and, therefore is the most expensive one in terms computer economy (memory and time).

5.2.2 Charge modeling

The second approach is in terms of charge modeling. Depending on the needed accuracy, the knowledge of the problem, and the time and computer available memory, there are several

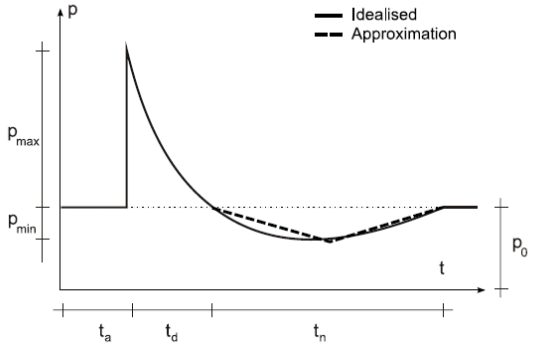

Figure 5.2: Pressure-time curve for a free air blast wave, see [3].

options (figure 5.3).

The first is the *Air Blast Wave model* (AIRB) [14] [15]. An idealized experimental results for free-air explosions is used in order to simulate an equivalent TNT charge explosion in the structures' faces. A modified Friedlander equation (5.1) is used for this porpoise.

$$p = p(m, d, t) \tag{5.1}$$

This method is computationally cheap and fast as the fluid is not taken into account. But on the other hand, reflections, shadowing, street channeling can not be modeled. In general, the AIRB works for simple geometrical situations.

The second way of modeling a explosive charge is by a *compressed air bubble*. The detonation is treated as a high difference of air pressure between the bubble and the surrounding air. This requires calibration and this procedure can be tedious as explained in the examples.

An last, a *solid TNT equivalent* may be used by Jones-Wilkins-Lee state equation. This is the best approach to the reality, but also the most expensive one. It requires a fine mesh for the fluid, so the needed memory is its major drawback.

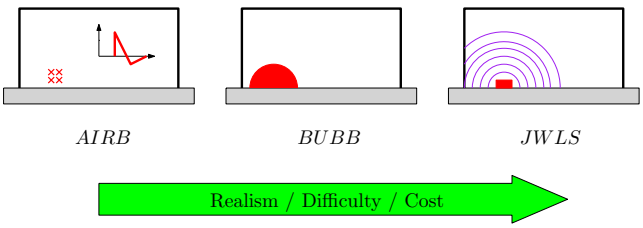

Figure 5.3: Comparison of the three ways to model the explosive charge.

Chapter 6

Contact-Impact between solids

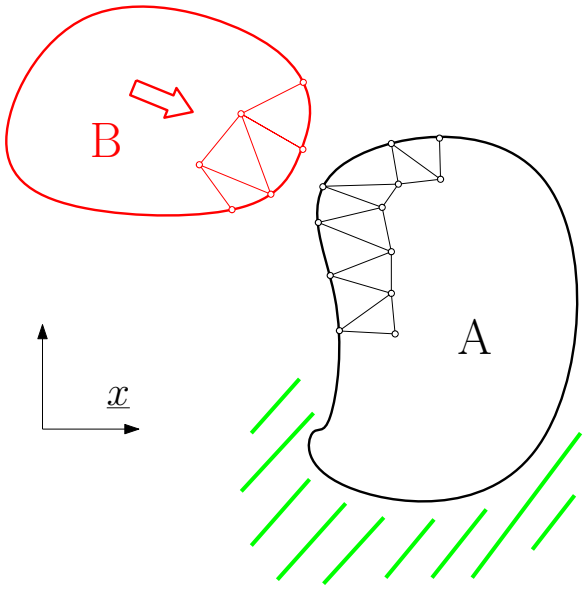

Figure 6.1: Lagrangian Contact-Impact description.

The classification of contact-impact between solids can be done as:

Slow It refers to slow loading, smooth contact and friction problems. Its study is specially useful for metal forming and shaping-manufacture industries.

Fast Impacts or crashes are the common problems concerning fast contact-impact. For fast loading, where friction is not too important; or large deformations with no fragmentation.

Very Fast complete failures and perforations are treated in this last contact-impact problems. Perforation is a special case that is going to be studied in a example.

There are lots of manners to solve contact-impact problems in the literature. All of the methods consist of two main components:

1. Contact detection module, in order to know whether the contact exists or not, and when happens. It is usually carry out by heavy geometrical computations.
2. A contact enforcement technique. For example, penalty or Lagrange multipliers.

Some of the main methods are the followings:

Conventional contact-impact methods The contact is detected by node-through-surface penetration. The method works with "slave" nodes and "master" surfaces. More information in referencia. Nevertheless, this techniques do not work well in certain circumstances. Normally problems occurs when the technique deals with strange geometries where contact detection turns tricky or with some ambiguous contact cases.

Pinball method This method consists on embedding an sphere in each element [16]. The contact between elements occurs when (see the figure (6.3)) the following inequation (6.1) becomes true:

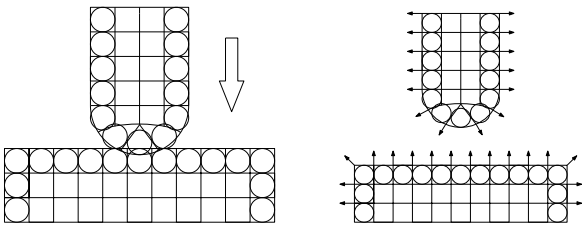

Figure 6.2: Pinball method description.

$$d_{12} < (R_1 + R_2) \tag{6.1}$$

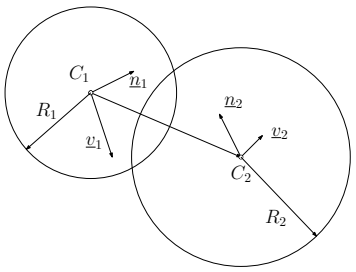

Figure 6.3: Contact between elements.

This method has also its shortcomings concerning slender and distorted continuum elements or with zero-thickness beam and shell elements.

So as to solve this problems, *The Hierarchic Pinball Method* was developed [17]. In this case a parent pinball is embedded in each element and recursively descendent pinballs are generated as long as contact holds.

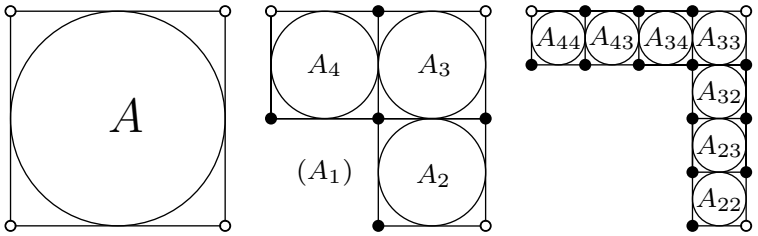

(a) Level 0 (b) Level 1 (c) Level 2

Figure 6.4: Descendent pinballs generation

When does hierarchy stop? It continues dividing each element until the minimum size or max level is reached for continuum elements or until the size equals physical element thickness in shell elements.

Smoothed Particles Hydrodynamics (SPH) The basic idea behind this methos is to represent a continuum by a set of particles, whose motion is governed by the conservation laws of continuum mechanics [18] [19].

It was developed in the 70s for astrophysical problems (Lucy, Gingold, Monaghan, 1977) involving the motion of compressible fluids in complex geometries. Its goal is to verify the behavior of the structure, and not so much concerned in the impacting body. Its applications are plenty, every phenomena described as an impact of a relatively soft body onto a structure, with or without fragmentation (aeronautics applications, nuclear impacts, etc.).

Formulation

The method is based upon the following identity (6.2) for a function f:

$$f\left(\underline{r}\right) = \int f\left(\underline{r}'\right) \cdot \delta\left(\underline{r} - \underline{r}'\right) \, dV \tag{6.2}$$

$\underline{r}$ = position vector $\qquad$ δ = Dirac's distribution
f = scalar vector field (ρ, $\underline{v}$...)

The equation (6.2) can be approximated by a regularization, using Kernel function $W(\underline{r}, h)$ where h is the characteristic length and W satisfies certain properties. So:

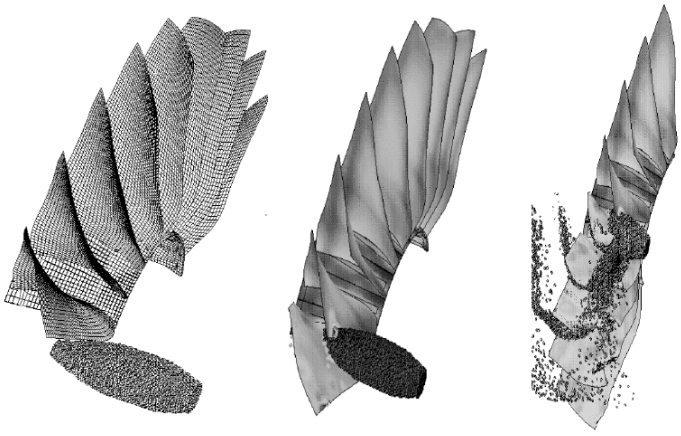

Figure 6.5: An application in aeronautics. Bird strike simulation. See [2].

$$f(\underline{r}) \approx \langle f(\underline{r}) \rangle = \int f\left(\underline{r}'\right) \cdot W\left(\underline{r} - \underline{r}', h\right) dV \tag{6.3}$$

To write the equations of continuum mechanics under the form of a particle approximation, it is necessary to estimate the various fields (density, energy, etc.) and their spatial gradients (gradient, divergence, ...). Then for each term one have to follow this steps:

1. Term of dynamic conservation equation at point $\underline{r}$.
2. Multiply by $W\left(\underline{r} - \underline{r}', h\right)$.
3. Integrate over the fluid domain with special attention to the boundaries.
4. Approximate the integrals by discrete summations.
5. Term of SPH equation at point $\underline{r}$.

As the approach is Lagrangian, it has the advantage of not using a mesh in the traditional sense, so that all problems related to excessive mesh distortions are avoided. It allows to overcome the limitations of classical FE-based methods and their drawbacks. SPH can also be effectively coupled with standard FE to model impact phenomena with fragmentation.

On the other hand there are some disadvantages, as the recalculation of connectivity at each step is costly or the weak treatment of the materials' laws. It is a quite "young" method so it is spected that improvements will complement SPH method.

Chapter 7

Examples

7.1 Parking

7.1.1 Objective

The objective of this example is the simulation of an explosion in a parking lot and the analysis of the structural response for different materials. The evolution of the pressure in the fluid will be also studied, as well as the influence of the meshing in the final results.

Different models of explosions' simulation are used, so as to compare them and decide which best represents the real problem. Approaches have been done in 2D and 3D.

First of all the model is described, where material characteristics, dimensions and constitutive laws are detailed. Then, the results are explained for the 2D and 3D cases, with the necessary figures and graphics in order to understand the conclusions properly. Finally, this results are discussed and compared with the intuitive physical behavior, and the results obtained by the

7.1.2 Model

The pre-process has been done with Cast3m and for the calculation EUROPLEXUS code has been used. In terms of post-process, the graphics have been drawn with Cast3m and Excel, and the movies with the EUROPLEXUS code.

As far as the fluid-structure interaction scheme is concerned, the non-structural failure hypothesis has been elected. Therefore, the geometrical mesh matching is conforming or non-conforming depending on the mesh refinement. On the other hand, strong mechanical coupling has been used in FE.

As far as the geometry of the structure is concerned, it has been summarized in the table 7.1.

Characteristic of the Structure	Dimension
Number of Stories	3 in 2D 1 in 3D
Number of Parcels	5 in 2D 1 in 3D
Plant height	3.2 m
Forged's thickness	0.4 m
Width between columns	14.4 m
Columns' width	0.8 m

Table 7.1: Geometry of the structure

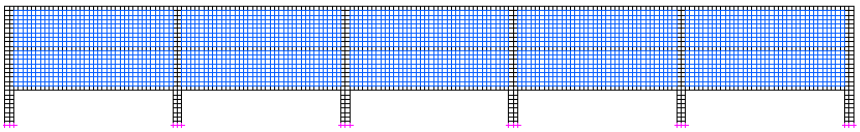

(a) 2D

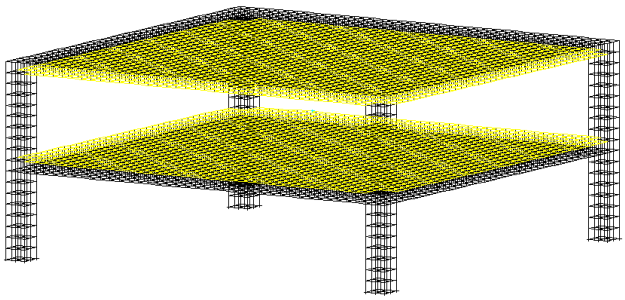

(b) 3D

Figure 7.1: Mesh of the structure in 2D and 3D.

In addition, the material used in each domain has its own characteristics and particularities (table 7.2). The structure has been represented by a linear elastic material, modified or not with a Mazars damage model for concrete (non-linear model) [20] [21].

In terms of fluid modeling, the explosion has been simulated in two ways: as a TNT charge equivalent (air blast wave) or by a difference of pressure, energy and air density in a

Type of material	ρ [kg/m^3]	E [Pa]	ν	f_c [Pa]	f_t [Pa]
Linear Elastic	2500	$3.4{\cdot}10^10$	0.2		
Mazars Non-linear	2500	$3.4{\cdot}10^10$	0.2	$30{\cdot}10^6$	$2.9{\cdot}10^6$

Table 7.2: Characteristics of the concrete

little fluid bubble. The characteristics for the fluid are specified in the table 7.3.

Type of material	ρ [kg/m^3]	E_{int}	γ
Air	1	$2.5{\cdot}10^5$	1.4
Explosion bubble	1500 for 3D and 200 for 2D	$5{\cdot}10^6$	1.4

Table 7.3: Characteristics of the fluid

The explosive has been located in the middle of the first floor, represented by a material point for the AIRB calculation, and by a suspended box (0.3x0.3x0.3 m) in the air for the FSA type. The ground has been treated as completely rigid and the movement of the base of the pillar blocked.

In order to achieve the objectives, different meshes combined with different types of elements and sizes (h_s for the structure and h_f for the fluid) and fluid-structure interaction approaches have been modeled. The table summarizes every test that has been made, for 2D and 3D.

As specified in chapter 5 there is a big deal referring to the comparison between air blast wave and the high pressure air bubble simulation. The relation is not straightforward and there are currently studies about the issue. For this report, a suitable change of pressure has been chosen for 2D and 3D cases in order to notice the structural response due to the charge.

7.1.3 Results

The experiments and the printed results have been carefully chosen so as to find the best physical representation, but also to clarify some ideas exposed in the previous chapters. The results appear divided in 2D and 3D, since there is a big computational difference for an extra dimension.

As shown in the figure 7.4 for 2D and 3D cases two approaches have been studied: the effect of the explosion in the structure using the AIRB TNT equivalent charge, and the total coupled fluid-structure problem with FSA.

The descriptive characteristics obtained vary with the different examples, but generally,

Dimension	FSI	Concrete	h_f [cm]	h_s [cm]	Element	CPU [s]
2D	AIRB 50 kg	Lineal	-	40	TRI	37.78
	AIRB 50 kg	Lineal	-	20	TRI	145.45
	AIRB 50 kg	Lineal	-	40	QUA	15.75
	AIRB 50 kg	Lineal	-	20	QUA	85.52
	AIRB 100 kg	Lineal	-	40	TRI	34.22
	AIRB 100 kg	Lineal	-	20	TRI	140.77
	AIRB 100 kg	Lineal	-	40	QUA	14.14
	AIRB 100 kg	Lineal	-	20	QUA	86.73
	FSA	Lineal	40	40	TRI	32.48
	FSA	Lineal	40	40	QUA	22.56
	FSA	Lineal	20	40	TRI	93.39
	FSA	Lineal	20	40	QUA	78.71
3D	AIRB 100 kg	Lineal	-	40	CUBE	7.16
	AIRB 100 kg	Lineal	-	20	CUBE	250.37
	AIRB 100 kg	Lineal	-	10	CUBE	370.39
	AIRB 100 kg	Lineal	-	5	CUBE	931.61
	AIRB 100 kg	Mazars	-	40	CUBE	25.22
	AIRB 100 kg	Mazars	-	20	CUBE	268.27
	AIRB 100 kg	Mazars	-	10	CUBE	1279.98
	AIRB 100 kg	Mazars	-	5	CUBE	2569.26
	AIRB 50 kg	Lineal	-	40	CUBE	5.31
	AIRB 50 kg	Lineal	-	20	CUBE	53.84
	AIRB 50 kg	Lineal	-	10	CUBE	249.98
	AIRB 50 kg	Lineal	-	5	CUBE	688.53
	AIRB 50 kg	Mazars	-	40	CUBE	17.84
	AIRB 50 kg	Mazars	-	20	CUBE	187.16
	AIRB 50 kg	Mazars	-	10	CUBE	840.75
	AIRB 50 kg	Mazars	-	5	CUBE	2398.31
	FSA	Lineal	40	40	CUBE	174.14
	FSA	Lineal	20	40	CUBE	3821.84
	FSA	Mazars	40	40	CUBE	214.69
	FSA	Mazars	20	40	CUBE	3716.83

Table 7.4: Summary of the models used

vertical displacement, Von Misses value, velocity field, fluid pressure and structural damage level (for the Mazars material) are shown.

2D

For the 2D, a control point has been established right down the location of the explosion, and its displacement measured, in order to compare different meshes and approaches.

The figure 7.2 and shows the displacements of the control point concerning the AIRB

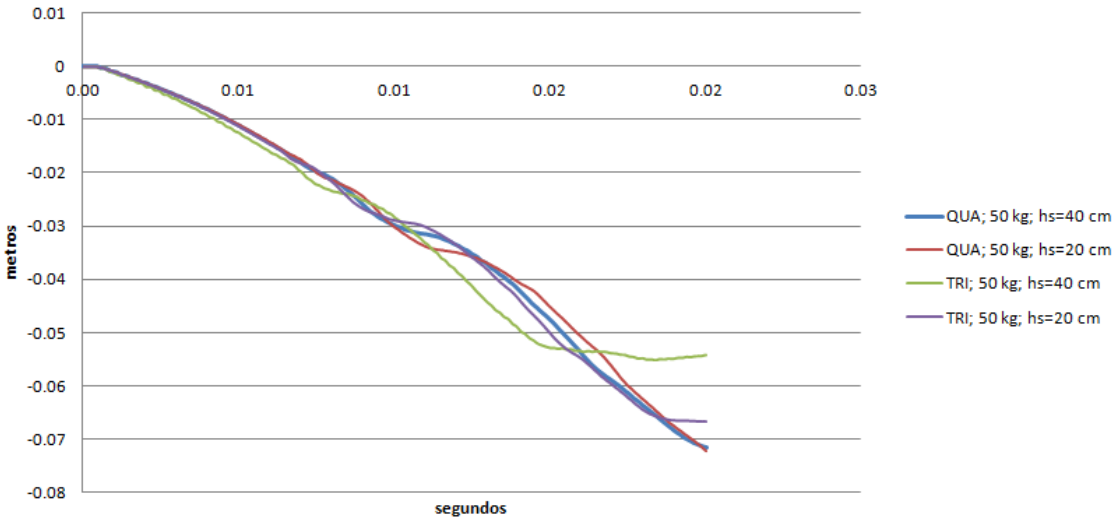

(a) 50 kg TNT

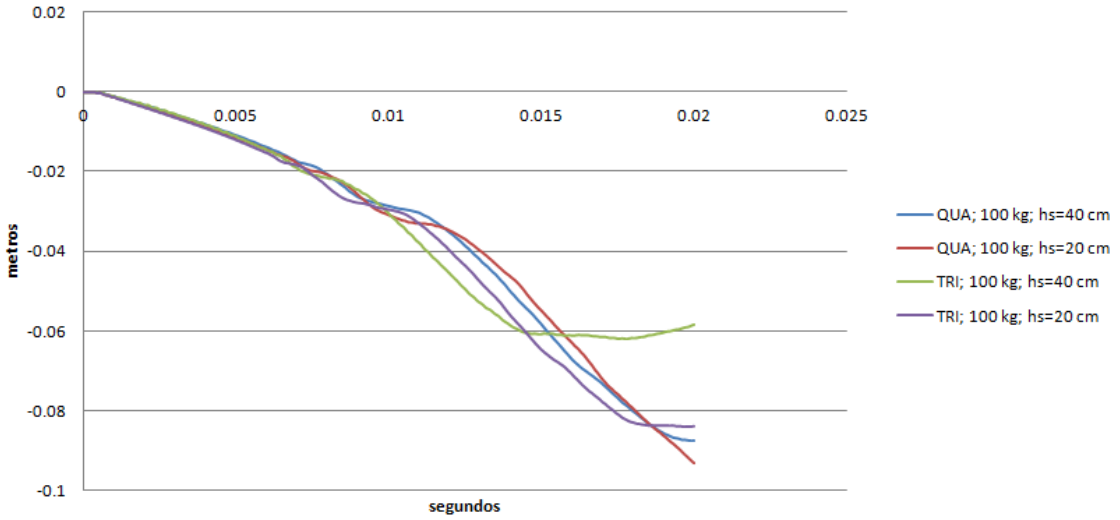

(b) 100 kg TNT

Figure 7.2: Vertical displacement of the control point, depending on the element for AIRB simulation

model, with 50 or 100 kg. of TNT equivalent charge, and different element types and sizes.

Some others factors have been analyzed such as the Von Misses Criterium equivalent or the instant nodal velocity. Since the structure is treated as Lagrangian, every element is attached to a material so the nodal velocity refers to the structure's motion velocity.

The best way to represent the evolution of those variables is by a movie. Those movies have been created and the figures 7.3 and 7.4 represents the behavior of the descriptive factors in time.

In order to study the fluid's behavior the whole fluid-structure interaction has been taken into account. This allows to obtain the air's pressure in every time step, which may be interesting to know in certain cases. As explained before the charge has been simulated by a difference of pressure between the bubble and the air. The value of the pressure difference has been chosen in such a way that the structural response is similar to that achieved with the previous AIRB model (figure 7.5). Then, the pressure in the air is represented in the figure 7.6

3D

As the 2D model is not enough to represents the reality, the 3D approach has to be performed. For the 3D, in addition to the linear material, an available Mazars model with damage is used. In consequence structural damage maps are obtained, which is much more interesting than any other descriptive variable. A control point is also fixed, the same point as before, the structural point just below the charge or the high-pressure bubble. The 2D approach helps in the election of the best element type, cubes in this case.

As in the 2D problem, the AIRB model has been computed with 50 and 100 kg of equivalent TNT charge, but for both materials. The figure shows all the results concerning the vertical displacement of the control point for every tested mesh.

This results may be better understand with a Von Misses Criterium and structural damage map for the Mazars material model (figures 7.9 and 7.10).

For a further analysis, the fluid has also been modeled. This turns the computation much more heavy, and the mesh refinement has been limited due to the lack of computer's available memory. In this case the fluid's pressure has been pointed out, as well as the Von Misses Criterium and damage map for the structure. Notice that for this calculation the charge has been approximated as a difference of pressures (figure 7.3).

A comparison of vertical displacement has also been made for every refinement level and material tested (figure 7.14)

7.1.4 Analysis of the results

2D

The problem in 2D has its own limitations. As far as the structural domain is studied alone, the general approach with the AIRB model gives coherent results. The internal way of computing the pressure in the structure's faces allows the code to impose pressure in every desired place. That is why the effect of the explosion arrives not only to the closest boundaries but also to the farest ones.

This can be easily sawn in the evolution of the nodal velocity, as the motion of the floor

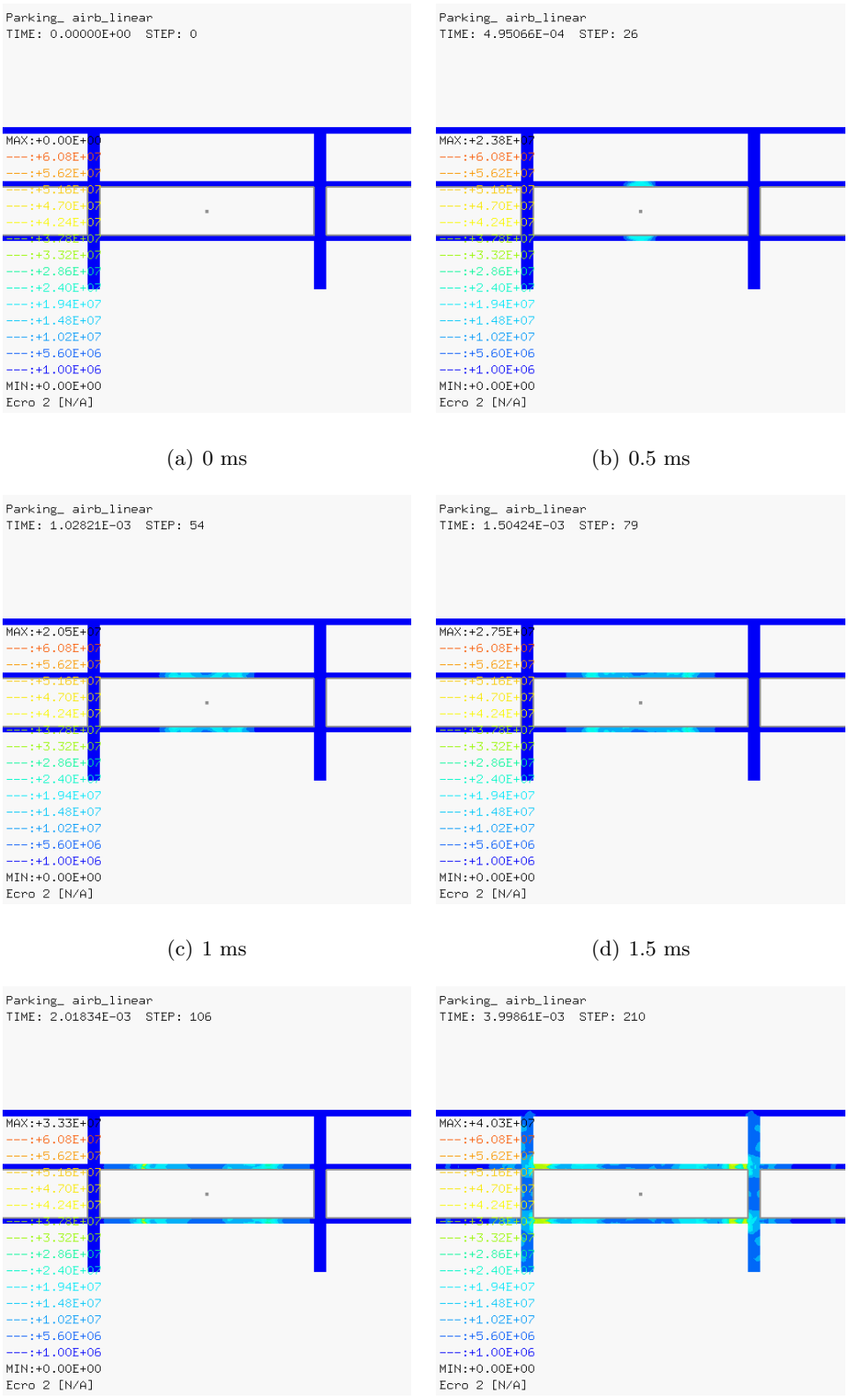

(a) 0 ms

(b) 0.5 ms

(c) 1 ms

(d) 1.5 ms

(e) 2 ms

(f) 4 ms

Figure 7.3: Von Misses Criterium for 100 kg TNT equivalent.

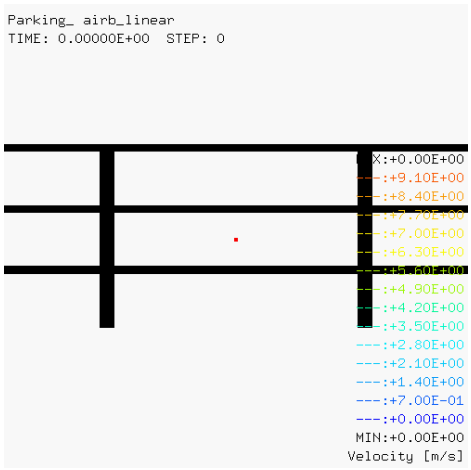

(a) 0 ms

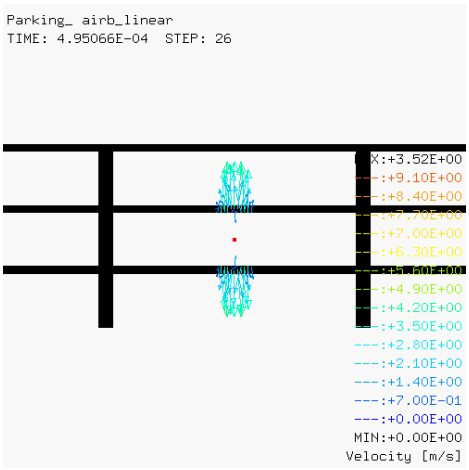

(b) 0.5 ms

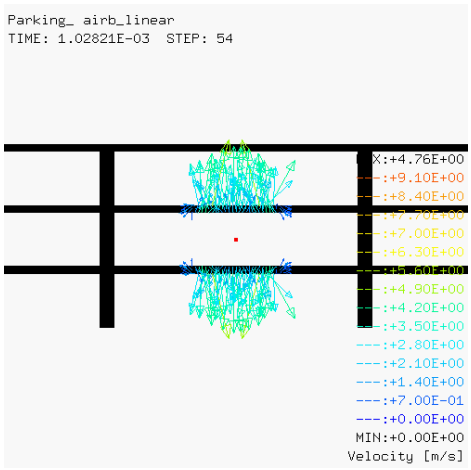

(c) 1 ms

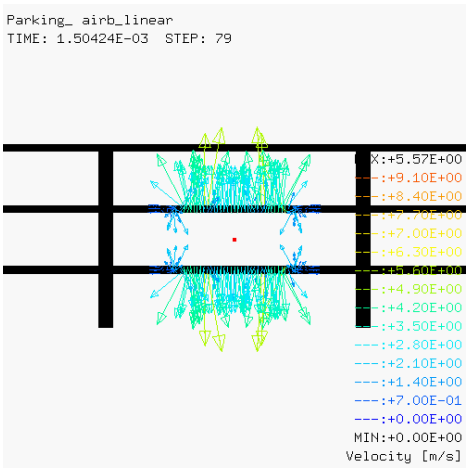

(d) 1.5 ms

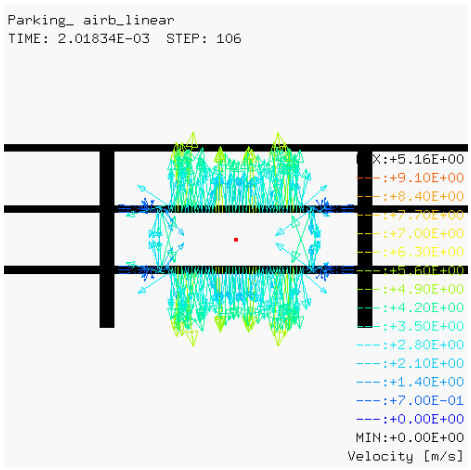

(e) 2 ms

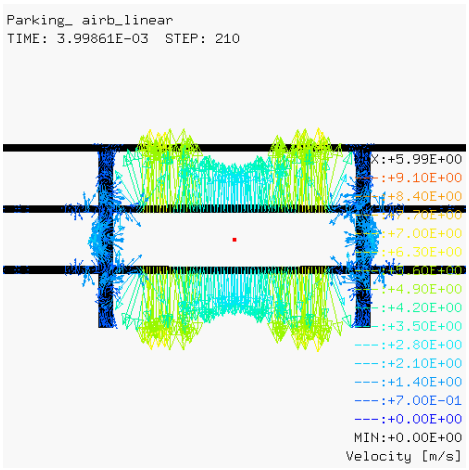

(f) 4 ms

Figure 7.4: Nodal Velocity for 100 kg TNT equivalent.

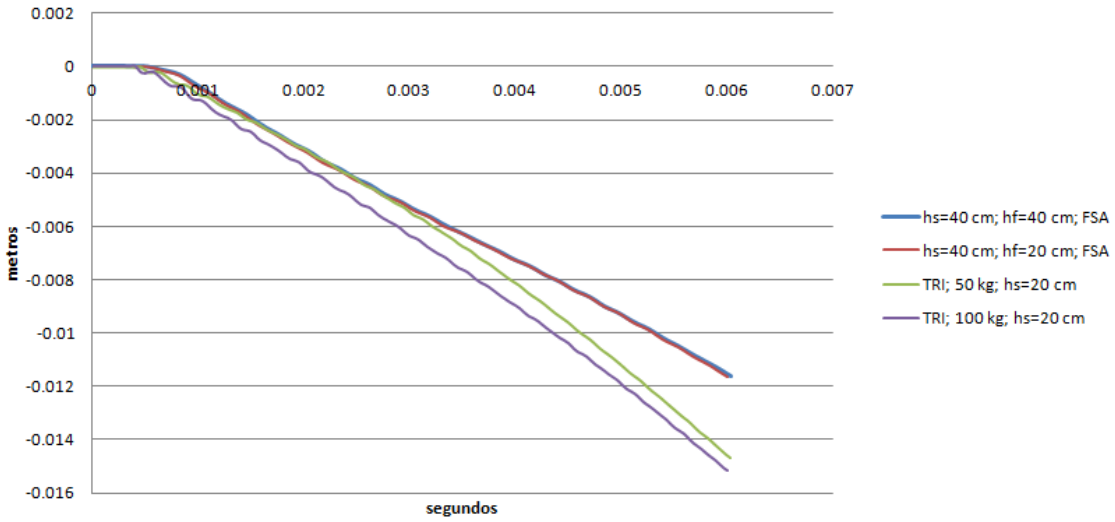

Figure 7.5: Comparison between the chosen pressure and previous AIRB simulations. Vertical displacement of the point of control.

slab of the neighbors compartments (not the square where the explosive is situated but the closest ones) is firstly generated because of the stiffness of the structure (goes up) and then once the explosive-wave arrives it goes down. In addition, if the vertical displacement of the control point is compared with the one obtained in the 3D, similar structural behavior is perceived.

But this does not happen in the second tried approach. Modeling the fluid in 2D means in this case that it is going to be confined inside the four "walls". Obviously, the reality is not well represented as the fluid remains inside the structure, as if in a infinitely long tunnel.

The importance of the meshing has been clearly proved. Not only a good refinement is needed but also the election of an adequate element is preferable. The figure 7.2 illustrates the variation that occurs depending on the refinement and the element type. Even though the FSA approach is useless in order to represent the reality, its representation has been helpful so as to see the behavior of a high-pressure-air-wave for different element types. In the figure 7.6 the lector can easily distinguish the non-symmetrical pressure expansion. This is due to the shape of the element. That is why in the next 3D approaches, only cubes have been used, and consequently, the high-pressure-air-wave has a symmetrical behavior (see figure 7.13).

It can be concluded that for a coarse mesh and without change of the material parameters the structure becomes stiffer, and that convergence is reached with smaller elements. This value can be obtained faster using suitable element types, and for this regular geometry

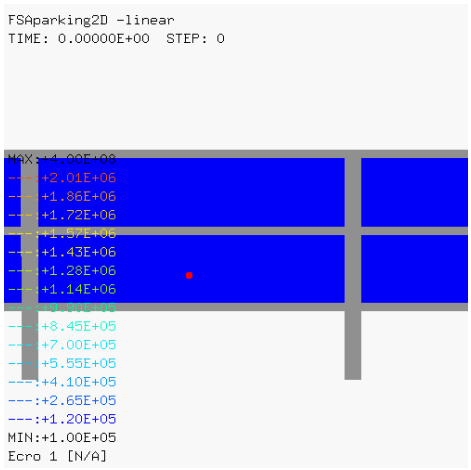

(a) 0 ms

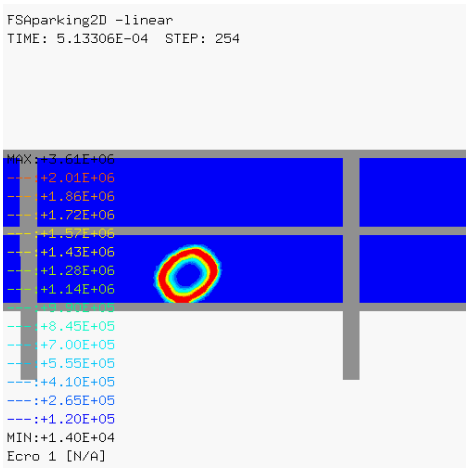

(b) 0.5 ms

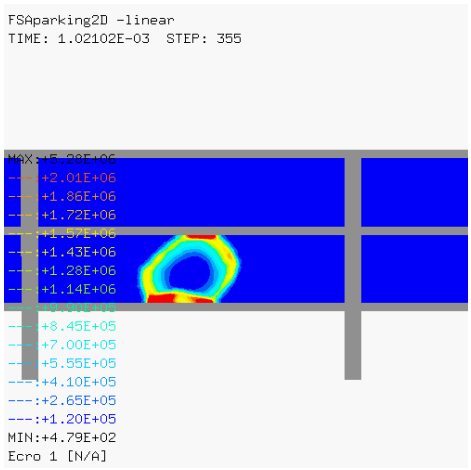

(c) 1 ms

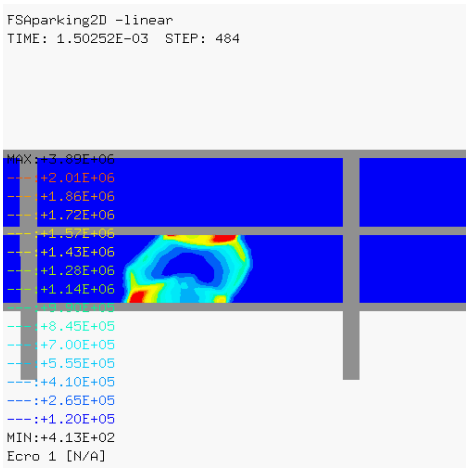

(d) 1.5 ms

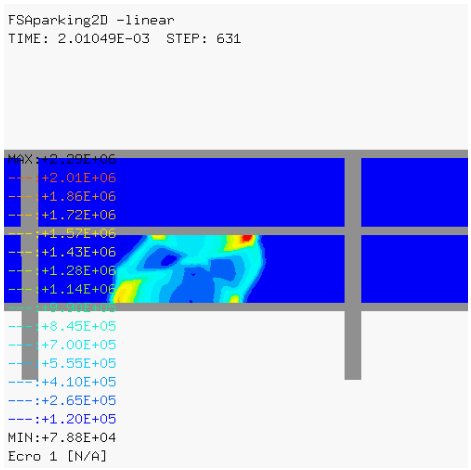

(e) 2 ms

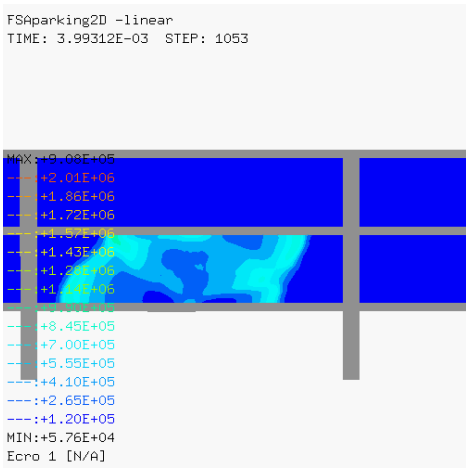

(f) 4 ms

Figure 7.6: Pressure of the fluid in Pa.

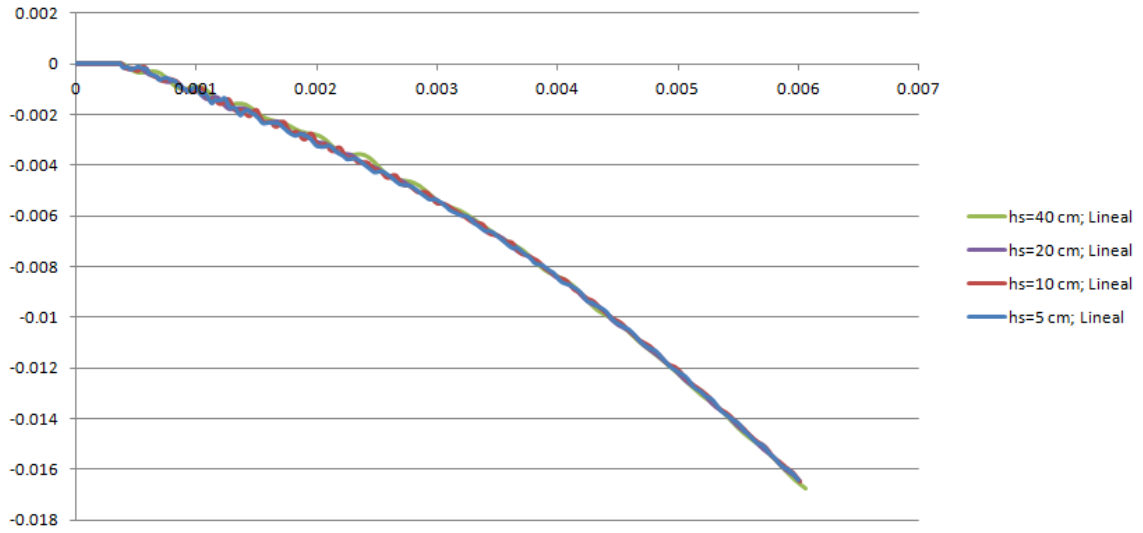

(a) 50 kg TNT for linear

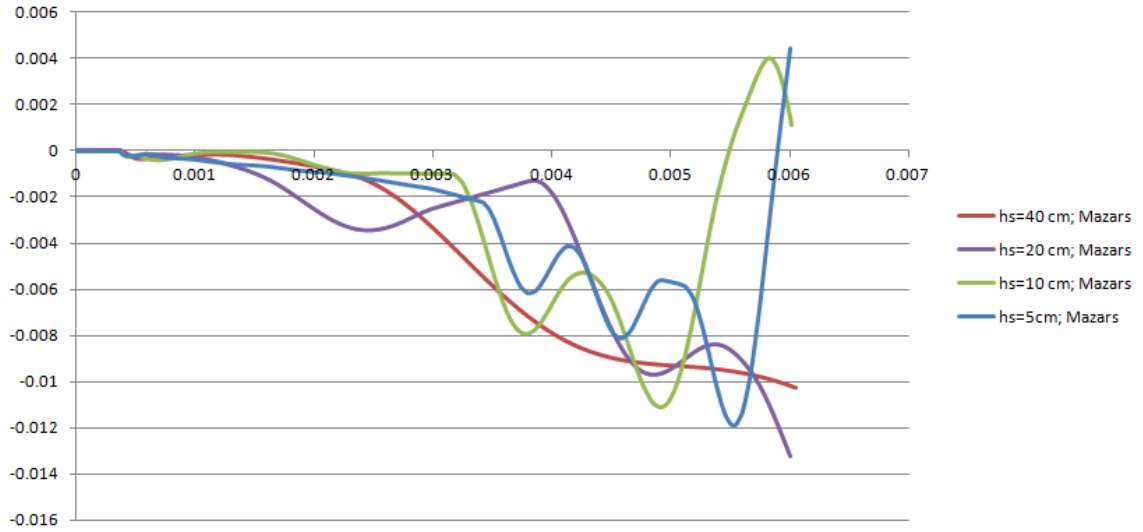

(b) 50 kg TNT for Mazars

Figure 7.7: Vertical displacement of the control point, depending on the element for AIRB simulation

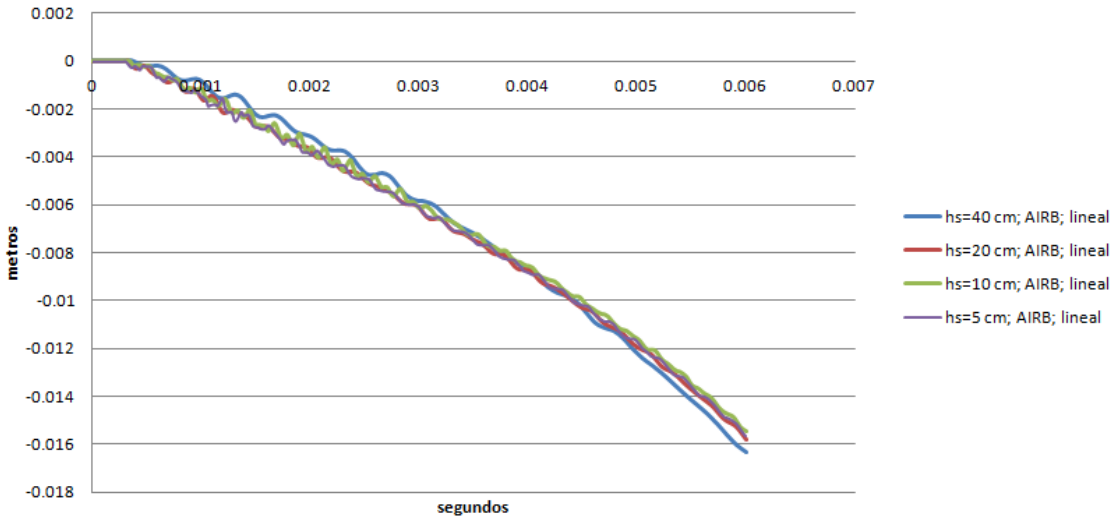

(a) 100 kg TNT for linear

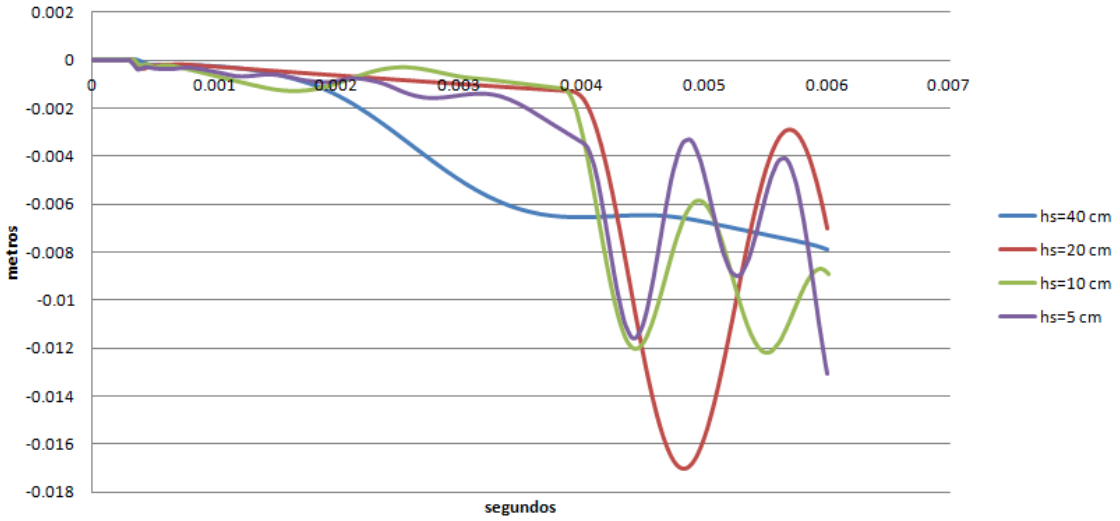

(b) 100 kg TNT for Mazars

Figure 7.8: Vertical displacement of the control point, depending on the element for AIRB simulation

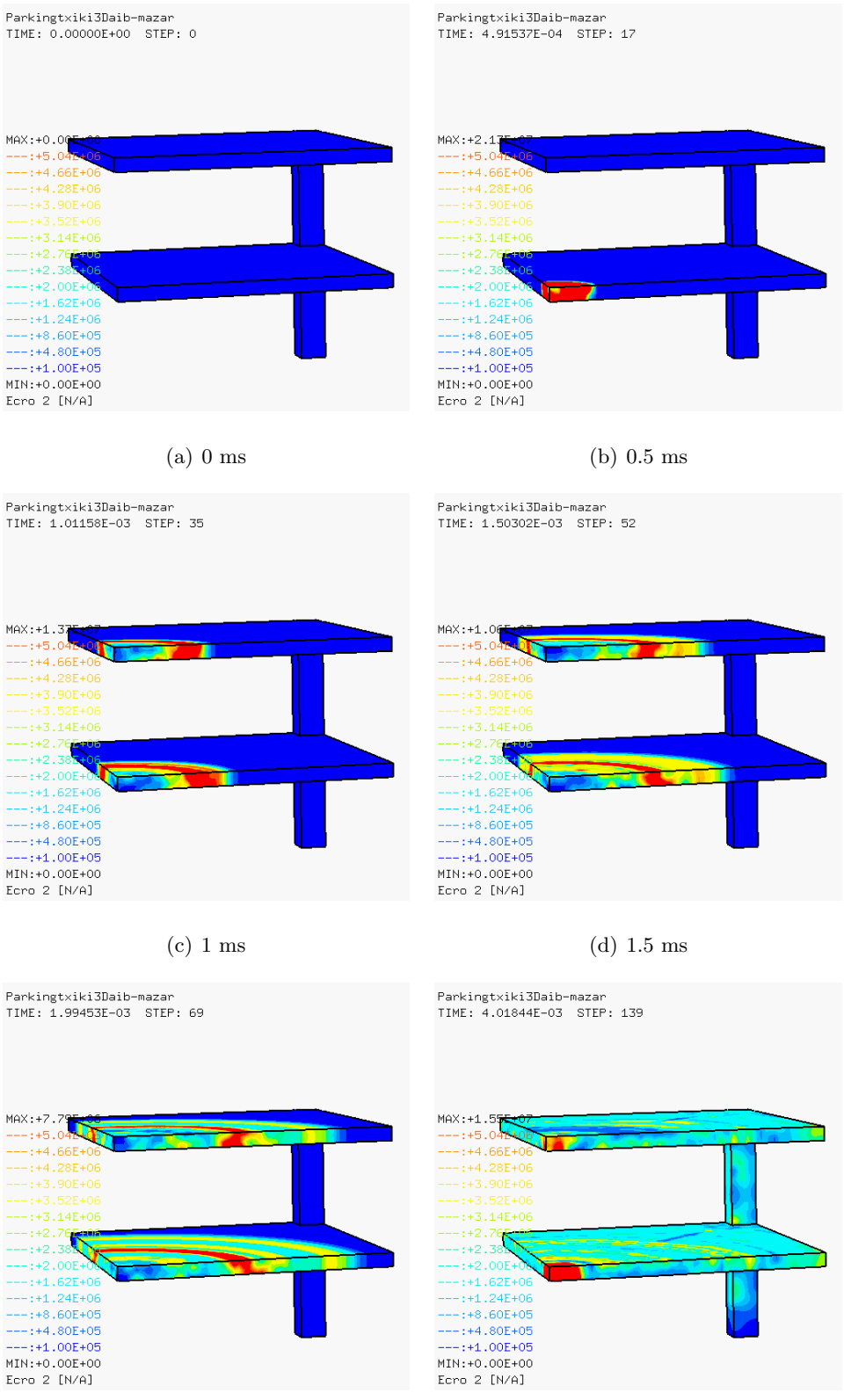

(a) 0 ms (b) 0.5 ms

(c) 1 ms (d) 1.5 ms

(e) 2 ms (f) 4 ms

Figure 7.9: Von Misses Criterium for 100 kg TNT equivalent

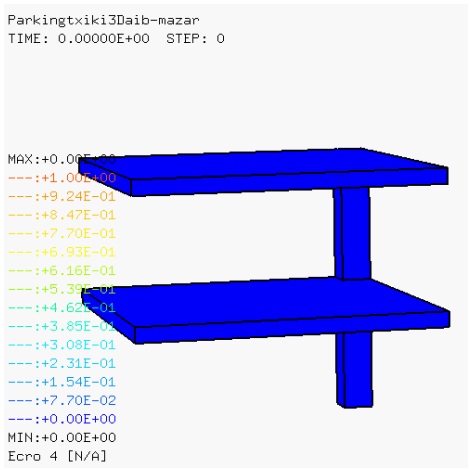

(a) 0 ms

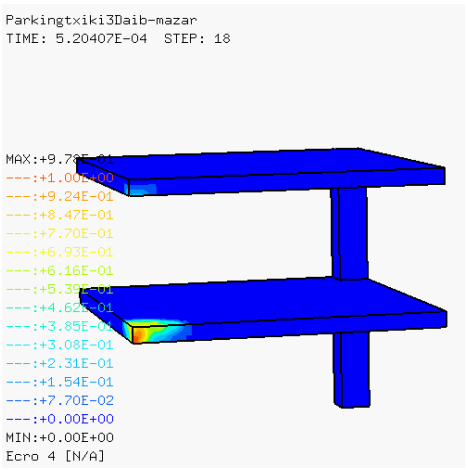

(b) 0.5 ms

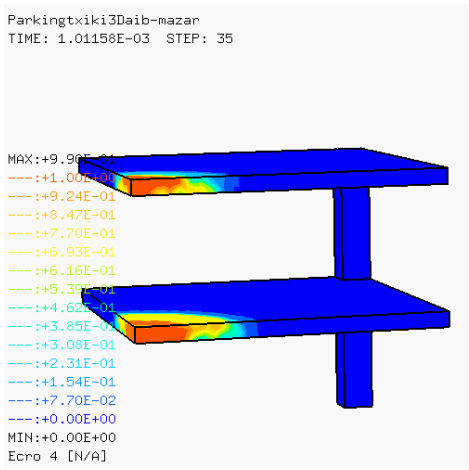

(c) 1 ms

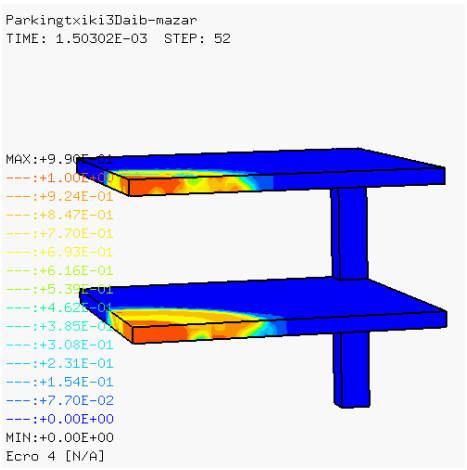

(d) 1.5 ms

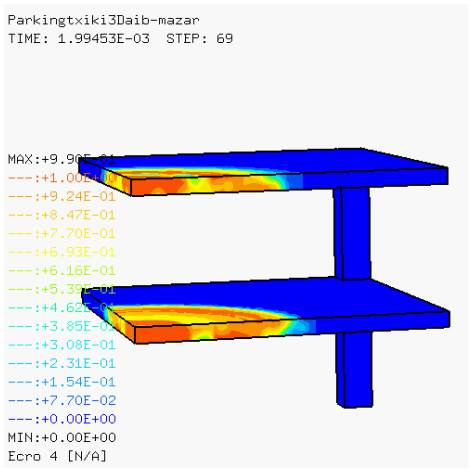

(e) 2 ms

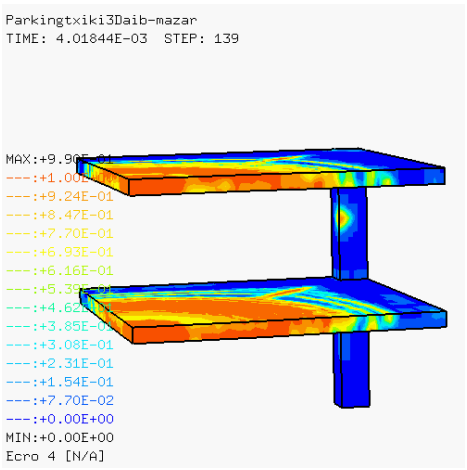

(f) 4 ms

Figure 7.10: Structural damage for 100 kg TNT equivalent

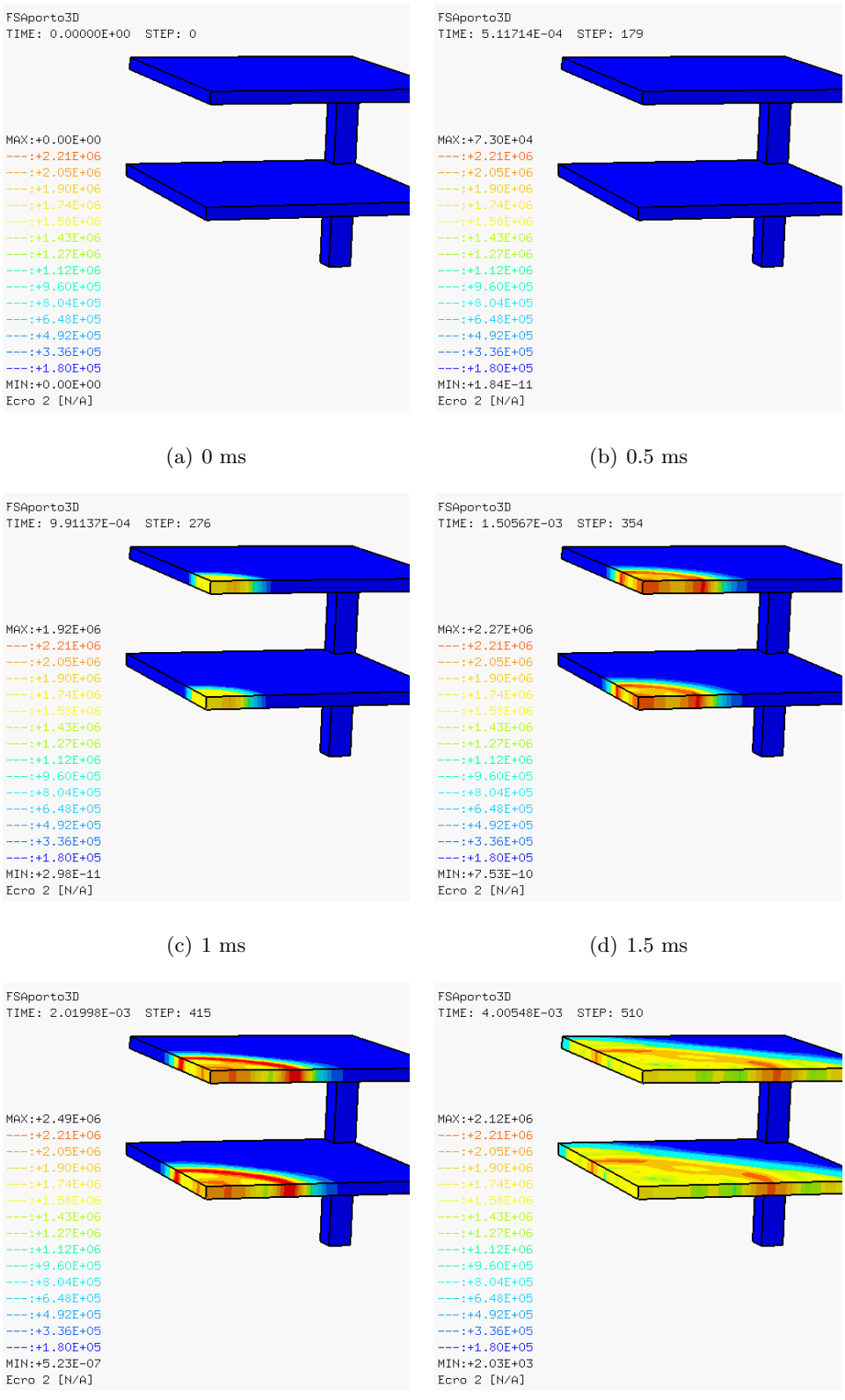

(a) 0 ms

(b) 0.5 ms

(c) 1 ms

(d) 1.5 ms

(e) 2 ms

(f) 4 ms

Figure 7.11: Von Misses Criterium for a high-pressure-air-bubble

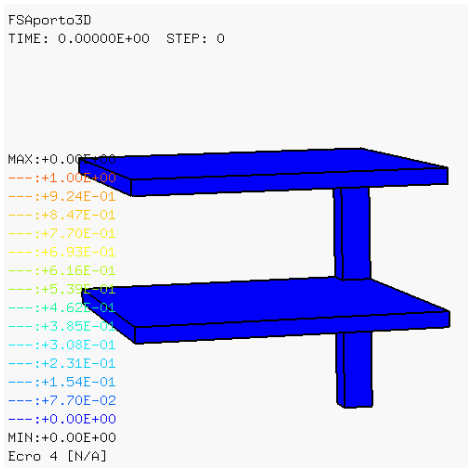

(a) 0 ms

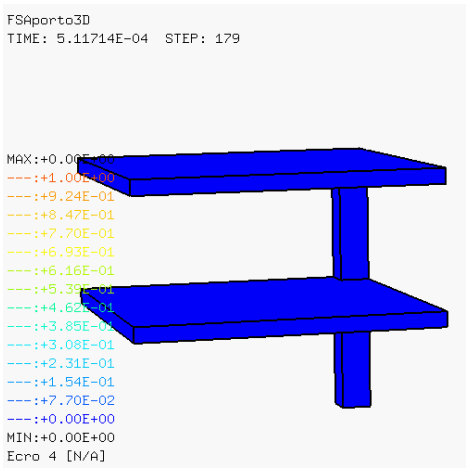

(b) 0.5 ms

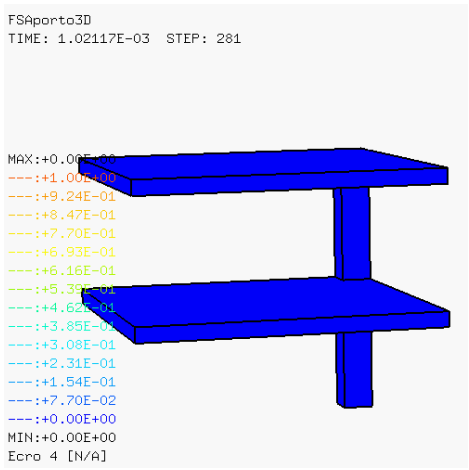

(c) 1 ms

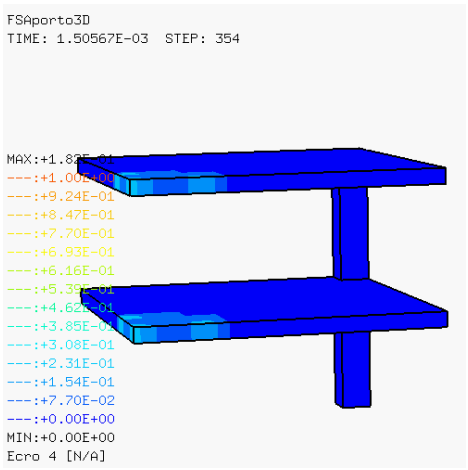

(d) 1.5 ms

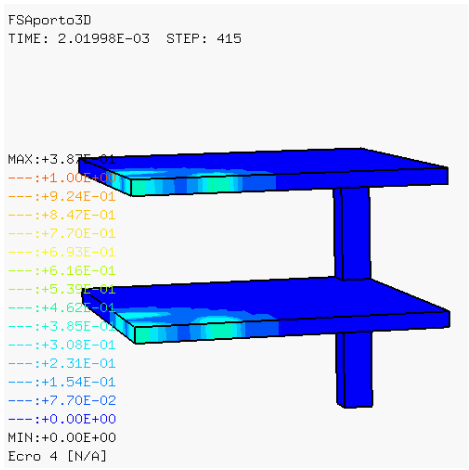

(e) 2 ms

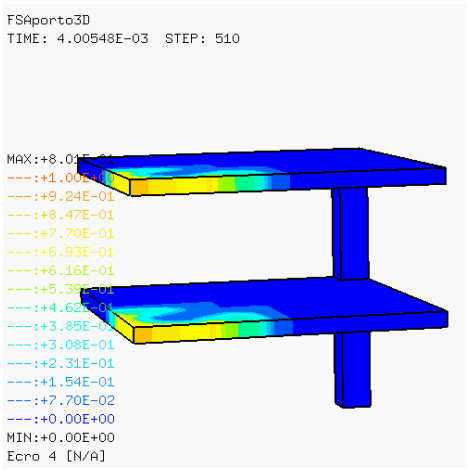

(f) 4 ms

Figure 7.12: Structural damage for a high-pressure-air-bubble

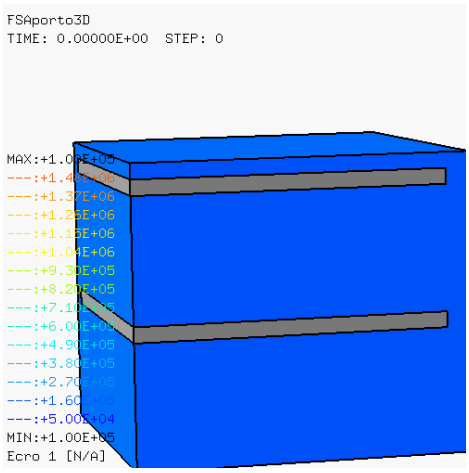

(a) 0 ms

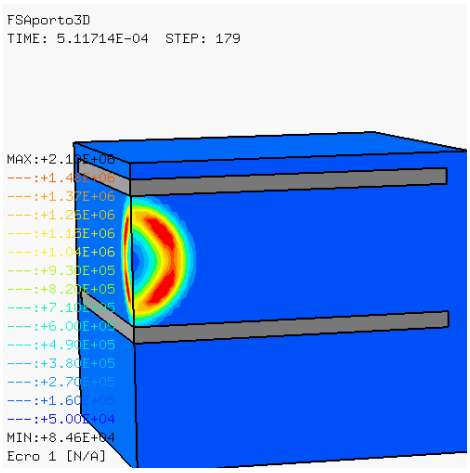

(b) 0.5 ms

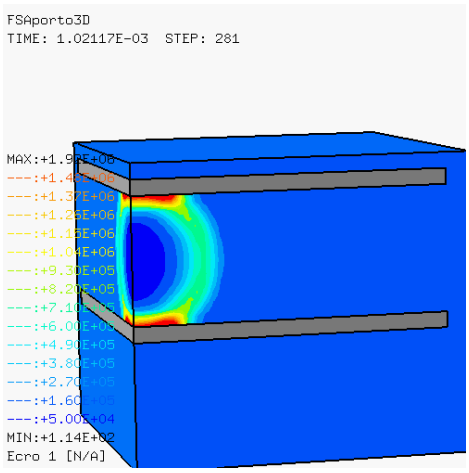

(c) 1 ms

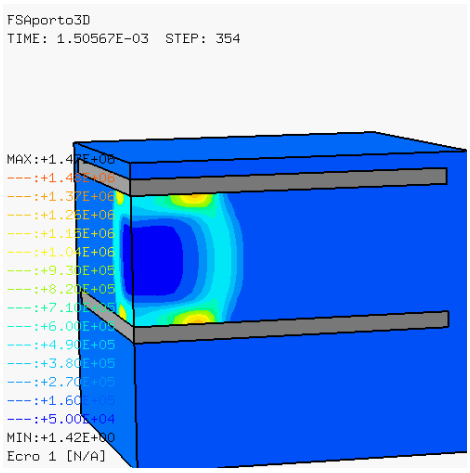

(d) 1.5 ms

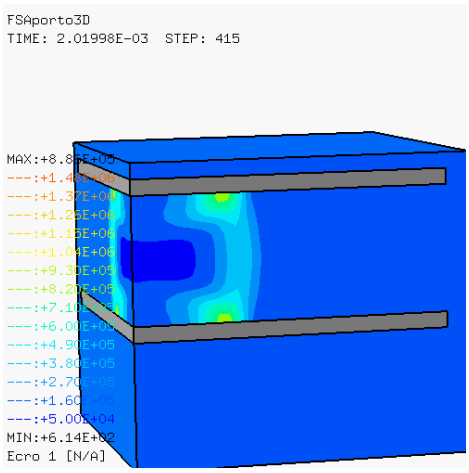

(e) 2 ms

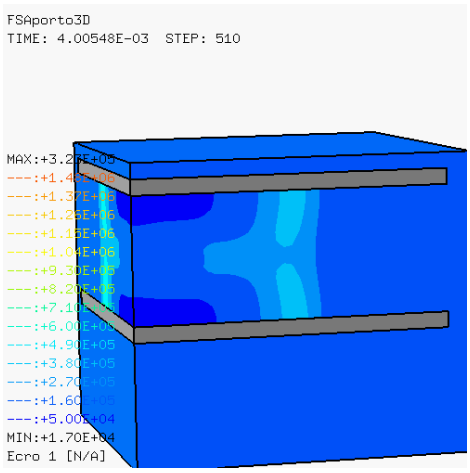

(f) 4 ms

Figure 7.13: Air pressure for a high-pressure-air-bubble

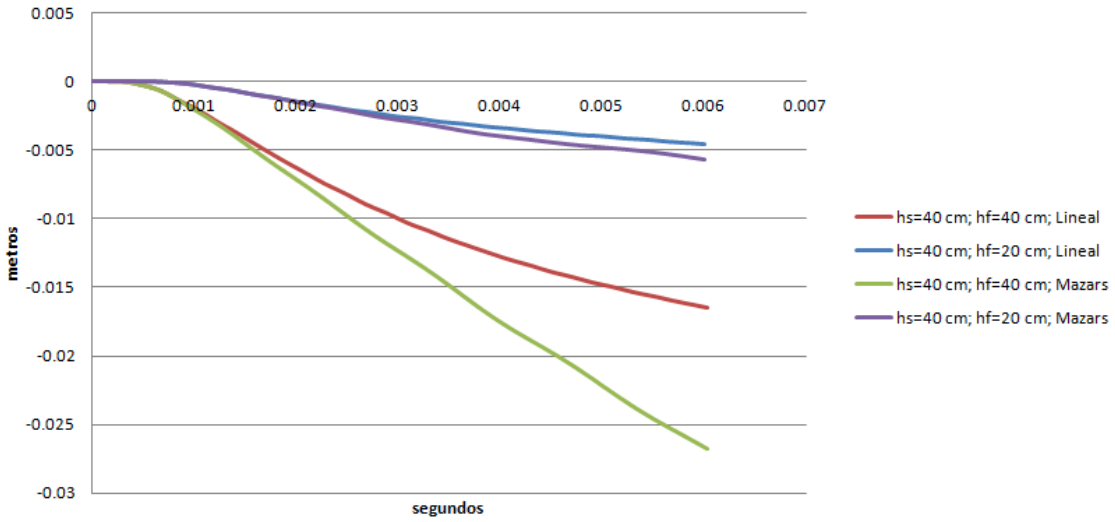

Figure 7.14: Comparison between mesh refinements and structural material. Vertical displacement of the control point.

square-shape ones seems the correct election.

3D

A 3D approach is completely necessary for this particular example. The 2D has been useful in terms of understanding generalities and different models' particularities, but unsatisfactory for a correct simulation. But it has also drawbacks, as the an extra dimension computation requires a huge amount of memory which has been a handicap in this minor thesis. Nevertheless, an accurate analysis of the results can be made.

The figures 7.7 and 7.8 show completely different structural behavior for both the linear concrete and the Mazars concrete model. This last model oscillates without control once reached a certain time, but the linear one does not. Without any additional information is difficult to understand why this may happen but the figure 7.10 gives a clue. The structure reaches the maximum damage level so the elements concerned are not longer useful for such a description. Furthermore, the same phenomena happens either for 50 kg TNT equivalent or for 100 kg TNT equivalent. As expected, both charges creates a full collapse in the structure, and the damage level reaches to the maximum level.

The mesh significance is not so important in those particular cases (specially for the linear material, see figures 7.7 and 7.8), due to the high charge. Nevertheless, refining the structural mesh may be acceptable, as it does not require such a big cost, and the movies can be played with higher detail.

Finally, the whole system has been analyzed. Figures 7.11, 7.12 and 7.13, represent the structure's response, as well as the fluid's pressure.

The first feedback to the figures is that the modeled pressure difference is not as powerful as the 100 or even the 50 kg of TNT equivalent. This allows a further study in the structural response in front of this charge, as it has not been completely collapsed. The explosion creates a little deflexion in the concrete because of the pressure generated by the blast wave. This creates compression in the structural faces exposed to the explosion, and traction in the external ones. What's more, this deflexion is higher where the stiffness is lower, so the regions distant from the pillars are those who would suffer the most. And this is exactly what shows the representation (figure 7.12). The damage is expanded symmetrically towards the parallels of the edges, as those are the weakest structural points.

The asymmetry described for the 2D disappears in the 3D case, as cubes have been used in the mesh generation (figure 7.13). Nevertheless, there is a big influence of the mesh refinement related with the high-pressure-air evolution. The pressure that reaches to the structure is lower with the mesh refinement (figure 7.14), so the structural response is closely linked with the fluid's element size.

7.2 Tank

7.2.1 Objective

The objective in this example is to model the impact of a bullet in a water filled metal tank. The consequences of this impact are going to be analyzed in both domains, the fluid and the solid, and their behavior shown for different initial speed and incidence angle.

7.2.2 Model

The used code is EUROPLEXUS, and the contact-impact system is treated with the pinball method Smoothed articles Hydrodynamics (SPH). That means that the system's representation is done by a set of particles and not by FE o FV. The material and geometrical characteristics are summarized in the tables 7.5, 7.6 and 7.7.

Object	Number of particles	Type of object	Model
Fluid	13902 particles	Isothermal, perfect	Euler
Tank	6062 particles	Elasto-plastic	Johnson-Cook, Lemaitre Damage [22]

Table 7.5: Characteristics of the objects

	ρ [kg/m^3]	C	P_0 [Pa]	P_{ref}
Water	1000	1450	10^5	10^5

Table 7.6: Characteristics of the fluid

	ρ [kg/m^3]	E [Pa]	ν	A [Pa]	B [Pa]	C [Pa]	n	$\dot{\bar{\varepsilon}}_0$	m
Tank	17600	$199{\cdot}10^9$	0.3	$175{\cdot}10^6$	$380{\cdot}10^6$	0	0.32	1	1

Table 7.7: Characteristics of the tank

The dimensions of the tank are the followings (table 7.8) and the figure 7.15 represents the steel-point-made-by mesh.

Characteristic	[cm]
Radio	15
Height	60
Thickness	1.5

Table 7.8: Projectile's initial conditions.

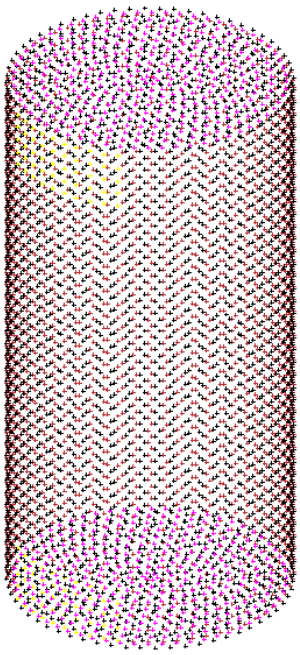

Figure 7.15: Mesh of the tank. Steel particles

The bullet is also discretized by particles but its characteristics are not important for this study. What happens with the projectile is not the case of study. The table 7.9 shows every tested approaches.

	Proj. init. speed [m/s]	Angle X axis [º]	Angle Y axis [º]	Angle Z axis [º]
1	1466	90	0	90
2	2932	90	0	90
3	2932	45	45	90

Table 7.9: Projectile's initial conditions.

7.2.3 Results

The structural damage equivalent (for Lamaitre model)(figure 7.16) and the water pressure (figures 7.17) are the main outputs given in this example. The case 2 has been fully developed, whereas for the third case only de deformation is printed (figure 7.18). The first case has been omitted as non-extra information may be given with it.

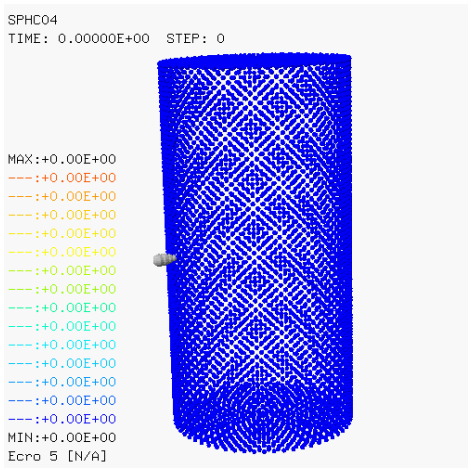

(a) 0 ms

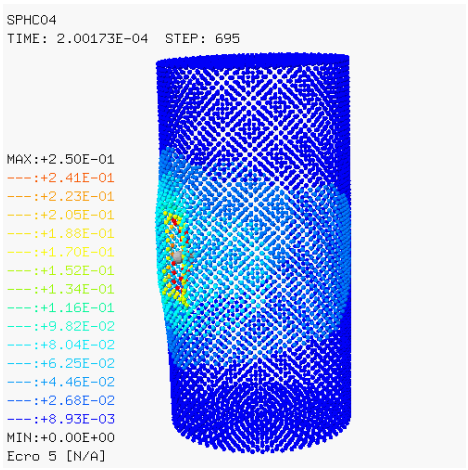

(b) 0.2 ms

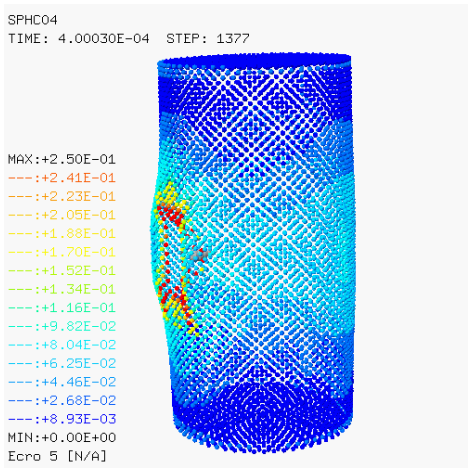

(c) 0.4 ms

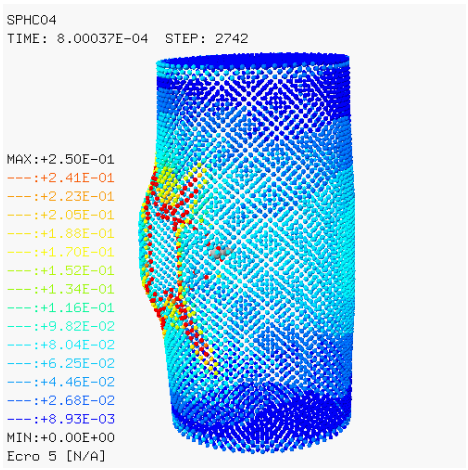

(d) 0.8 ms

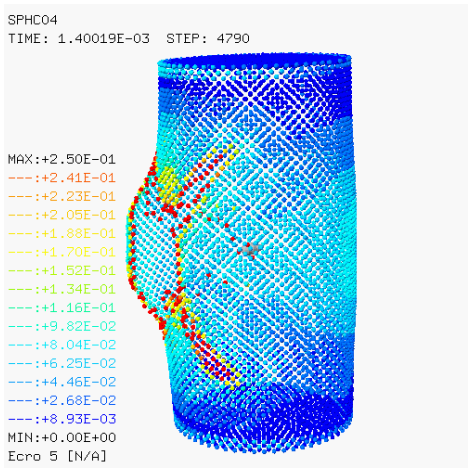

(e) 1.4 ms

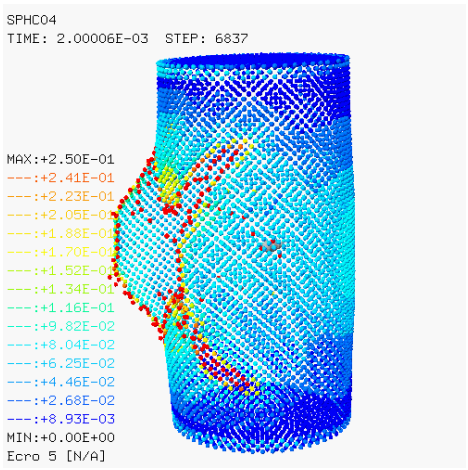

(f) 2 ms

Figure 7.16: Steel's damage and perforation. Case 2.

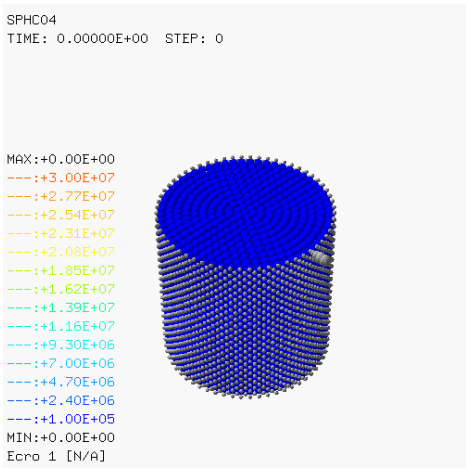

(a) 0 ms

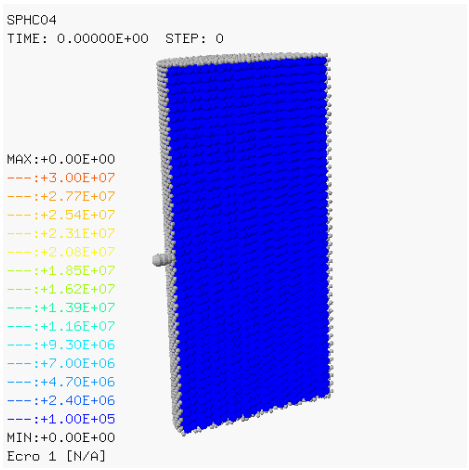

(b) 0 ms

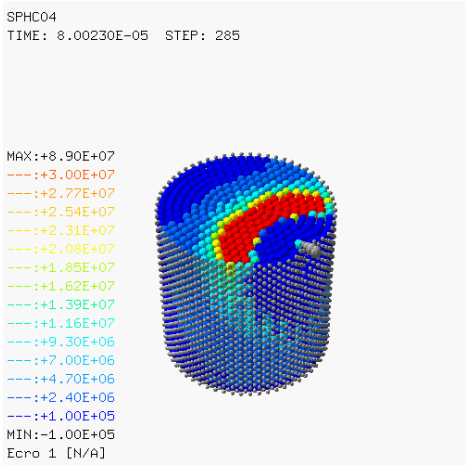

(c) 0.08 ms

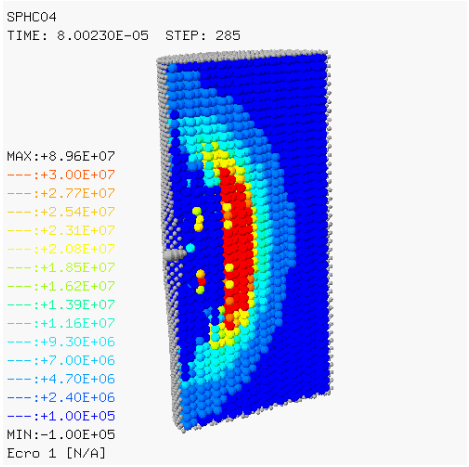

(d) 0.08 ms

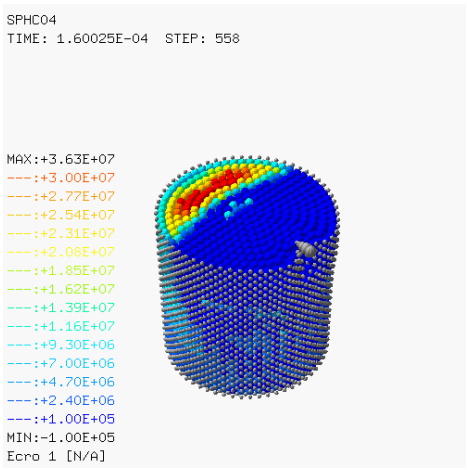

(e) 0.16 ms

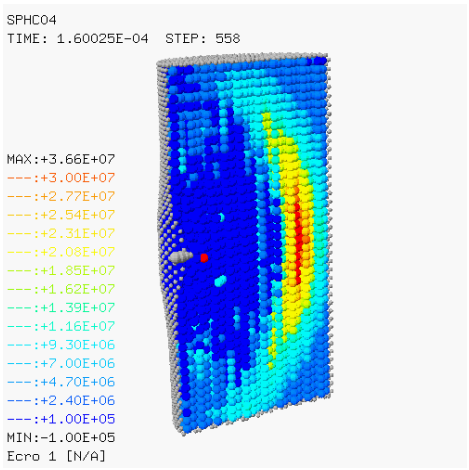

(f) 0.16 ms

Figure 7.17: Fluid's pressure. Case 2.

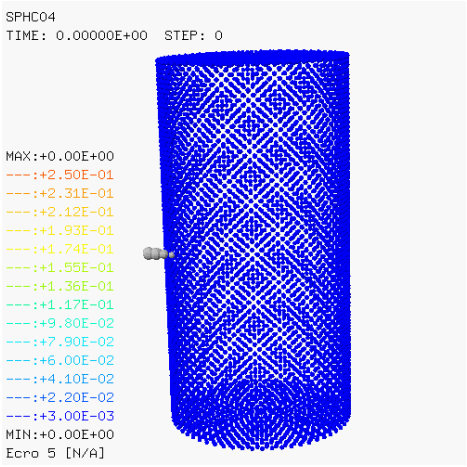

(a) 0 ms

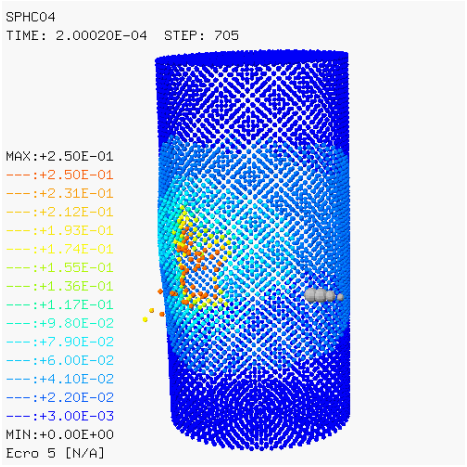

(b) 0.2 ms

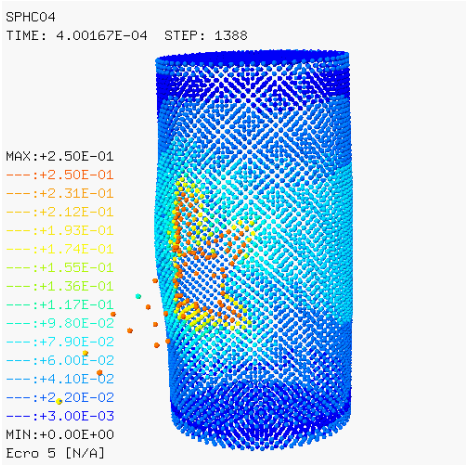

(c) 0.4 ms

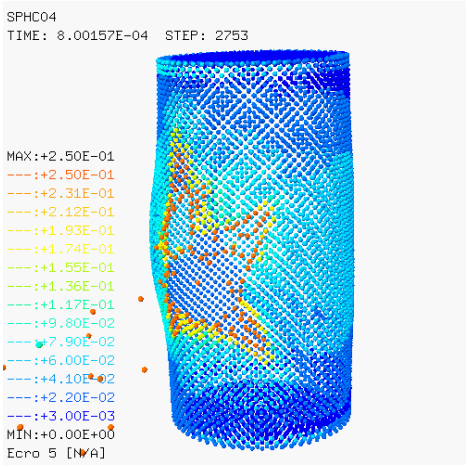

(d) 0.8 ms

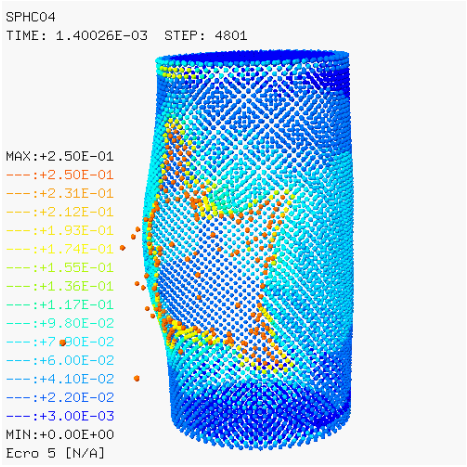

(e) 1.4 ms

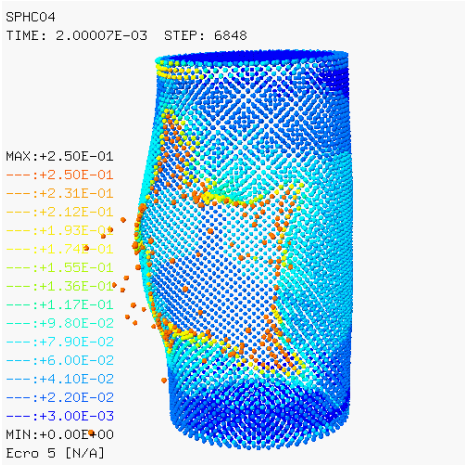

(f) 2 ms

Figure 7.18: Steel's damage and perforation. Case 3.

7.2.4 Analysis of the results

The model represents the reality. The structural fragmentation, perforation and expansion occur as expected. In addition, the tank is opened outwards, due to the pressure exerted by the fluid in the metallic wall. Literature states that the generated petaling depends upon the projectile's impact velocity and the lubrication. All the examples are equally lubricated but the difference of the initial conditions of the bullet (table 7.9) generate those shapes.

As for the fluid's pressure, the figure 7.17 shows the perfect symmetry of the expanded pressure, and how it is dissipated because of the deformation of the container, and because the water starts to exit by the drilling.

Chapter 8

Conclusions

Once the analysis of the examples has concluded, it is interesting to summarize the advantages and drawbacks that have been observed so far, so as to take them into account in future applications. Two different applications have been designed. Both examples are completely different in terms of the technique used to solve them, but they are good enough tests to draw conclusions of FSI functioning. The examples are:

- An explosion in a parking lot.
- Impact of a bullet in a water filled metal tank.

Firstly, when working with a real simulation is important to keep in mind what the limits of the employed model are. In the parking 2D example for instance. the easiest test to compute, has showed that the fluid's behavior is not the expected, and that the reality was not represented properly, not because of a numerical fault, but due to the own limitations of the model. Moreover, the AIRB was expected to behave worse than the model with the FSI, but it has shown its strength in this particular 2D example. Understanding the way the pressures are expanded and run in a particular model becomes the key to the success.

Then, once clarified and chosen a certain work pattern, is equally vital to know which are the variables that are going to be studied, or the required information. For instance, if a damage map is desired as an output, the structure should be modeled by a specific material. This type of material usually fixes the element to use in the meshing, so a simple decision of the material election determines some decisions from the beginning. Having those things in mind enables to ease the calculus, making suitable hypothesis if necessary and constructing the example correctly from the beginning.

In addition, taking into account all the decisions, the reality must be properly characterized. The first example shows the influence of the taken initial hypothesis in order to compare different models (in the 3D approach), or even same models with different refinement levels. The accuracy obtained will be closely linked with the correct parametrization of the problem. Nevertheless, in spite of a nice characterization of the system, there is also another limitation: computational requirement. There is a huge jump between 2D a 3D

problems in terms of needed computational memory. Whereas for 2D problems the elements' size has been reduced up to 5cm, this has been impossible for the 3D problems as observed in the table 7.4. The lack of computational memory is double in those problems because firstly the mesh have to be generated, and then, the code has to be run. The difference of the obtained results is best observed in figure 7.14.

Finally, the effectiveness of the SPH method has been proved in the second example. It allows to overcome the limitations of the classic FE-based methods in problems where a constant mesh topology becomes a serious drawback. Comparing it with the formulations explained in this thesis (Lagrangian, Eulerian and ALE), the SPH method gathers all the advantages of them, but goes further as there are not problems with mesh rezoning, boundary conditions are easily treated, and only the real domain is modeled. This relatively young method seems that is going to be a powerful and useful way of computing fast transient FSI problems in the near future. Nonetheless, for coarse particles it is difficult to distinguish the real behavior of the material yet, mainly due to the particle size, and the difficulty concerning the representation of material laws.

Bibliography

[1] In J. Donéa, editor. *Transient Response by Time Integration.* Applied Science Publisher, 1978.

[2] Universitat Politècnica de Catalunya. *Numerical Simulation od Fast Transient Dynamic Phenomena in Fluid-Structure Systems. Presentation slides and trace of proposed exercises/examples*, May 2011.

[3] Martin Larcher. Simulation of the effects of an air blast wave. Technical report, JRC European Comission, 2007. PUBSY JRC41337-2007.

[4] F. Casadei and J.P. Halleux. Binary spatial partitioning of the central-difference time integration scheme for explicit fast transient dynamics. *Int. J. Numer. Meth. Eng.*, 78:1436–1473, 2009.

[5] N.M. Newmark. A method of computation for structural dynamics. *J. Eng. Mech. ASCE*, 85:67–94, 1959.

[6] M.L. Wilkins. Calculation of elastic-plastic flow. methods of computational physics. *Academic Press*, 3, 1964.

[7] G. Jaumann. Geschlossenes system physikalischer und chemischer differentialgesefze. 120:385–530, 1911.

[8] A.E. Green and P.M. Naghdi. A general theory of an elastic-plastic continuum. *Arch. Rat. Mech. Anal.*, 18:251–281, 1965.

[9] P.L. Roe. Approximate riemann solvers, parameter vectors and difference schemes. *J. Comp. Phys.*, 43:357–372, 1981.

[10] Folco Casadei and N. Leconte. Fluid.structure interaction with cell-centered finite volumes in europlexus. Technical report, JRC European Comission, 2009. JRC53799.

[11] Folco Casadei and N. Leconte. Flsw: A weak, embedded-type fluid structure interaction model with ccfv in europlexus. Technical report, JRC European Comission, 2011. JRC65826.

[12] S. Giuliani. An algorithm for continuous rezoning of the hydrodynamic grid in arbitrary lagrangian-eulerian computer codes. *Nucl. Engng Des.*, 72:205–212, 1982.

[13] F. Casadei and J.P. Halleux. An algorithm for permanent fluid-structure interaction in explicit transient dynamics. *Comput. Meth. Appl. Mech. Eng.*, 128 (3-4):231–289, 1995.

[14] Martin Larcher and Folco Casadei. Explosions in complex geometries - a comparison of several approaches. Technical report, JRC European Comission, 2010. EUR 24288 EN - 2010.

[15] Martin Larcher and Folco Casadei. Explosions in complex geometries-a comparison between approaches. *Int. J. Protective Structures*, 1, 2010.

[16] Ted Belytschko and Mark O. Neal. Contact-impact by the pinball algorithm with penalty and lagrangian methods. *Int. J. Num. Meths. Eng.*, 31, 1991.

[17] T. Belytschko and I.S. Yeh. The splitting pinball method for contact-impact problems. *CMAME*, 105:375–393, 1993.

[18] R.A. Ginglod and J.J. Monaghan. Smoothed particle hydrodynamics: theory and application to non-spherical stars. *Mon. Not. R. Astron. Soc.*, 181:375–389, 1977.

[19] J.J. Monaghan. Smoothed particle hydrodynamics. *Annu.Rev.Astrophys*, 30:543–574, 1992.

[20] Jacky Mazars. *Aplication de la mécanique de l'endommagement au comportament non linéire et à la rupture du béton de structure.* PhD thesis, Université Pierre et Marie Curie - Paris 6, 1984.

[21] Yann Chuzel-Marmot. *Caractérisation expérimentale et simulation numérique d'impacts de glace à haute vitesse.* PhD thesis, Université MEGA de Lyon - INSA Lyon, 2009.

[22] G.R. Johnson and W.H. Cook Zhu. A constitutive model and data for metals subjected to large strains, high strain rates, and temperatures. *Proc. 7th Int. Symp. Ballistics, The Hague, The Nederlands*, pages 1–7, 1983.